Engineering Journal

Second Quarter 2024 | Volume 61, No. 2

Smarter. Stronger. Steel.

Engineering Journal

American Institute of Steel Construction

Dedicated to the development and improvement of steel construction, through the interchange of ideas, experiences, and data.

Engineering Journal (ISSN 0013-8029) is published quarterly. Published by the American Institute of Steel Construction at 130 E Randolph Street, Suite 2000, Chicago, IL 60601.

Lateral Force Distributions in Braced-Moment Frames

RALPH M. RICHARD, ERIC KELDRAUK, and JAY ALLEN

ABSTRACT

Braced frames intended to resist wind and seismic loads traditionally have been analyzed and designed as trusses with all joints modeled as pins, such that only the braces provide lateral force resistance. However, frames with gusset plate connections create a rigid joint zone between frame beams and columns, effectively resulting in moment frame behavior, particularly at larger drift angles when braces have yielded or buckled. Described herein are the force distributions for buckling-restrained braced frames (BRBF) subjected to story drift angles, where the lateral resistance of the frame comprises both brace and moment frame action.

Keywords: force distribution, buckling restrained braced frames (BRBF), braced-moment frame.

INTRODUCTION

Braced frames are typically modeled and designed as pinned connected truss members, wherein all lateral resistance is provided by the braces. The design of the gusset plates is subsequently based upon only the transfer of the brace forces to the pin connected beams and columns [*Vertical Bracing Connections—Analysis and Design*, Design Guide 29 (Muir and Thornton, 2014)]. This design rationale has proven acceptable for buckling-restrained braced frames (BRBF) story drift angles at and below that which induces yielding in the braces. However, at story drift angles of approximately 0.0025 (1/400) rad, the braces yield, as shown in the single-story frame pushover analysis in Figure 1, and additional lateral displacement is resisted by moment frame action (Walters et al., 2002). Designers of braced frames often ignore the moment frame action or mitigate it by introducing simple or semi-rigid connections in the braced frame [AISC *Seismic Provisions* Commentary Section F2.6b (2022a)]. Described herein is a rationale that evaluates the moment frame action of the braced frame to lateral loads after the braces yield.

Ralph M. Richard, Professor Emeritus, University of Arizona, Tucson, Ariz. Email: ralph@u.arizona.edu (corresponding)

Eric Keldrauk, Structural Engineer Analyst, Schuff Company, Phoenix, Ariz. Email: eric.keldrauk@gmail.com

Jay Allen, Executive Vice President of Engineering, Schuff Company, Phoenix, Ariz. Email: jayallense@yahoo.com

Paper No. 2022-12R

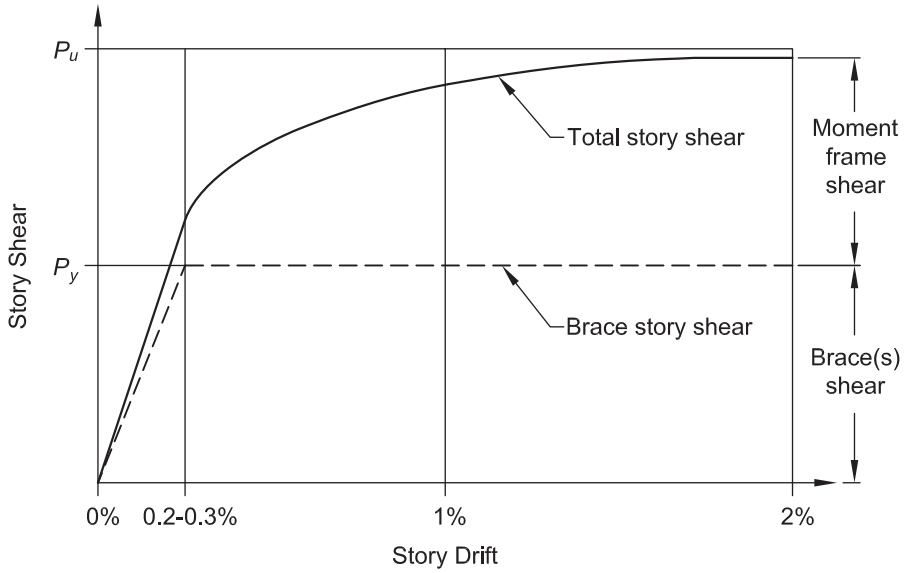

Fig. 1. Typical story shear distribution in a braced frame pushover analysis.

Shown in Figure 2 is a braced frame with typical force distributions using the equivalent lateral force method given in ASCE/SEI 7, *Minimum Design Loads and Associated Criteria for Buildings and Other Structures* (2022). At approximately 0.0025 (1/400) rad, the frame behavior transitions from an idealized braced frame to a combined braced-moment frame, schematically shown in Figure 3, with moment frame resistance resulting from the rigidity of gussets at the beam-column connections. The gusset plates serve a dual purpose of providing a rigid connection joint in addition to transferring the brace force to the beams and columns (Mahin and Patxi, 2002).

Braced-Moment Frame Design Rationale 1: Beam Hinge Mechanism

Figure 4(a) shows a braced-moment frame modeled for analysis of the seismic force distribution as a combination of the force distributions in a braced frame (b) and a moment frame (c). The force distributions in the frames shown in (b) and (c) are based on a seismic drift displacement that results in yielding of the braces in frame (b) and inelastic action in the top and bottom beams in frame (c) based on strong column-weak beam frame design. The forces in frame (b) are based on a pinned truss model with the braces at their yield.

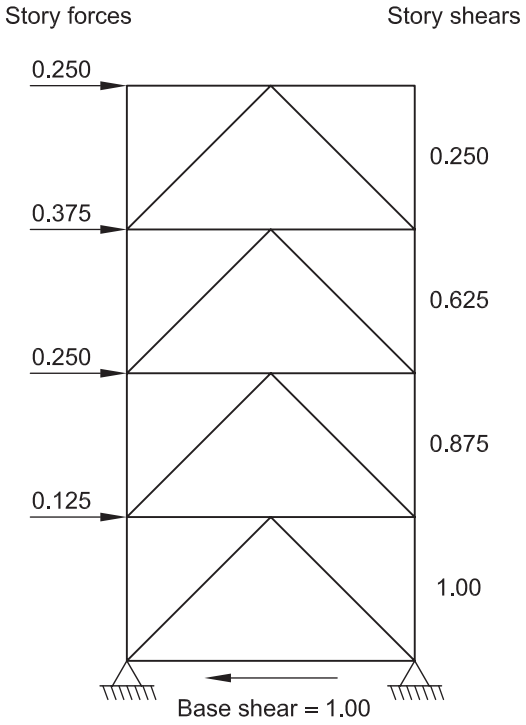

Fig. 2. Typical seismic force distribution in a braced frame using the equivalent lateral force procedure.

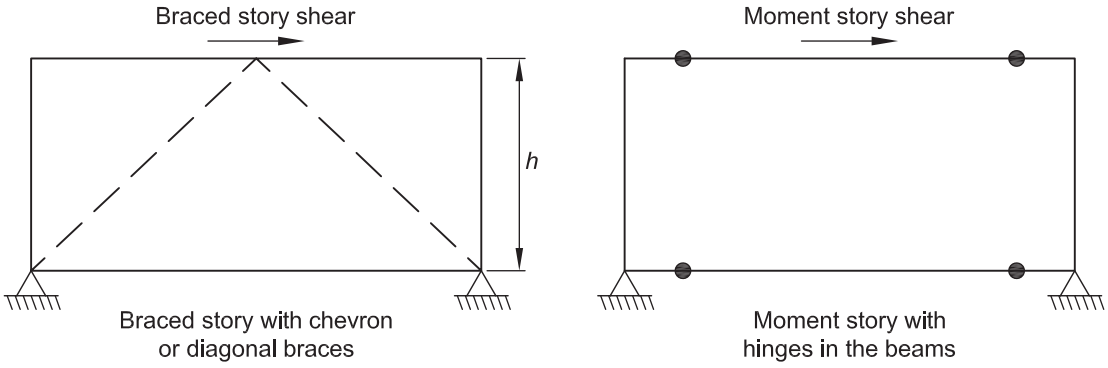

Fig. 3. Idealized single-story braced and moment frames for combined frame model.

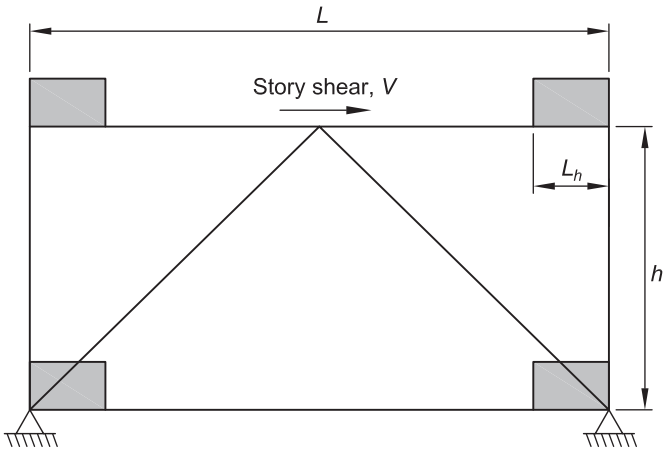

(a) Braced-moment frame

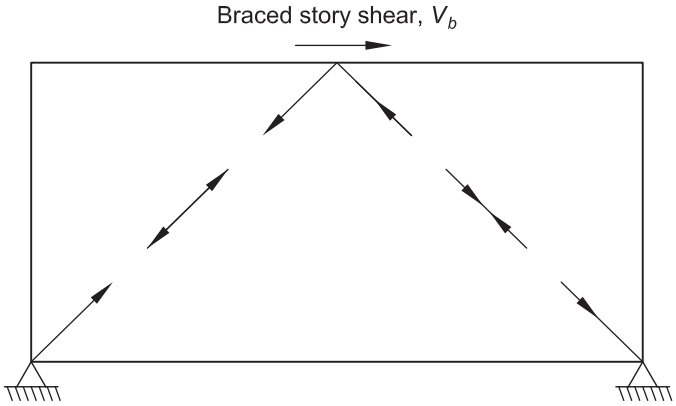

(b) Braced frame

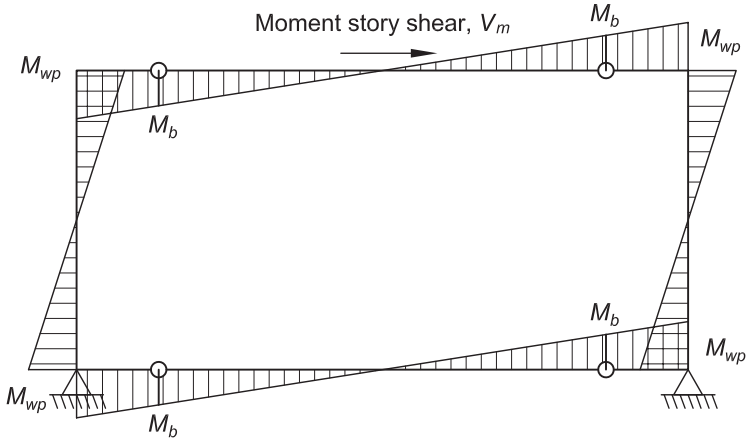

(c) Moment frame force distributions

Fig. 4. Braced-moment frame modeled for analysis of the seismic force distribution as a combination of the force distributions in a braced frame and a moment frame.

The inelastic action in frame (c) is modeled as a four-hinged frame with the hinges located in the beams at the ends of the gusset plates as shown. For a story drift of Δ, the story moment frame shear, V_m may be determined using the virtual work equation by equating external virtual work to internal work:

$$V_m\Delta = 4M_b\theta_{hinge} \tag{1}$$

where M_b is the beam hinge plastic moment, and θ_{hinge} is the hinge rotation.

The plastic hinge rotation in terms of the story drift angle, θ, is:

$$\theta_{hinge} = \theta k_1 = \frac{\Delta k_1}{h} \tag{2}$$

where the constant k_1 is defined in Appendix A and h is the story height.

The beam hinge plastic moment, M_b, is determined as follows:

$$M_b = M_u k_2 \tag{3}$$

where k_2 is a material term that adjusts the pure bending plastic hinge moment, M_u, to account for axial-moment interaction. The derivations of k_1 and k_2 are presented in the appendix of this paper.

Combining the previous equations gives the story shear for the moment story frame (c).

$$V_m = \frac{4M_u k_1 k_2}{h} \tag{4}$$

Referencing Figure 4 and knowing the moment frame story shear, V_m, the brace frame story shear, V_b, is determined as:

$$V_b = V - V_m \tag{5}$$

where V is the frame story shear. The design of the braces is based upon their expected yield stress. This rationale provides the forces in the braces, beams, and columns to design the gusset plates based on a braced-moment frame force distribution.

Braced-Moment Frame Design Rationale 2: Column Hinge Mechanism

Figure 5(a) shows a braced-moment frame modeled for analysis of the seismic force distribution as a combination of the force distributions in a braced frame (b) and a moment frame (c). The force distributions in frames (b) and (c) are based on a seismic drift displacement that results in yielding of the braces in frame (b) and inelastic action in the columns and top beam in frame (c).

The inelastic action in frame (c) is modeled as a four-hinged frame with two hinges located in the column at the end of the bottom gusset plates and two hinges located in the top beam at the ends of the gusset plates as shown. For a story drift of Δ, the story moment frame shear, V_m, may be determined using the virtual work equation by equating external virtual work to internal work:

$$V_m\Delta = 2M_b\theta_{h,b} + 2M_c\theta_{h,c} \tag{6}$$

where M_b is the beam hinge plastic moment, and θ_h is the hinge rotation.

The plastic hinge rotations, $\theta_{h,b}$ and $\theta_{h,c}$, in terms of the story drift angle, θ, are:

$$\theta_{h,b} = \theta k_{1,b} = \frac{\Delta k_{1,b}}{h} \tag{7}$$

$$\theta_{h,c} = \theta k_{1,c} = \frac{\Delta k_{1,c}}{h} \tag{8}$$

where the constants $k_{1,b}$ and $k_{1,c}$ are member specific (see Appendix A for derivation) and h is the story height.

The beam hinge plastic moment, M_b, and column hinge plastic moment, M_c, are determined as follows:

$$M_b = M_{u,b}k_{2,b} \tag{9}$$

$$M_c = M_{u,c}k_{2,c} \tag{10}$$

where $k_{2,b}$ and $k_{2,c}$ are member-specific material terms that adjust the pure bending plastic hinge moments, $M_{u,b}$ and $M_{u,c}$, to account for axial-moment interaction. The derivations of k_1 and k_2 are given in Appendix A.

Combining equations gives the story shear for the moment frame (c).

$$V_m = \frac{2}{h}\left(M_{u,b}k_{1,b}k_{2,b} + M_{u,c}k_{1,c}k_{2,c}\right) \tag{11}$$

Referencing Figure 5 and knowing the moment frame story shear, V_m, the brace frame story shear, V_b, is determined using Equation 5:

$$V_b = V - V_m \tag{5}$$

where V is the frame story shear. The design of the braces is based upon their expected yield stress. This rationale provides the forces in the braces, beams, and columns that are then used to design the gusset plates based on a braced-moment frame force distribution.

Comparison of the Beam-Moment Frame Analysis with Finite Element Analysis

Figure 6 shows the single-story frame used for comparative results. The beams are W21×101, the columns are W14×176, the braces are buckling-restrained braces (BRBs) with a core area of 6 in.^{2}, and the gusset plates are 18 in. × 18 in. Frame members and plates are ASTM A992/A992M (ASTM, 2020) material with F_y = 54 ksi and

ν = 0.30 (Poisson's ratio). The ANSYS finite element analysis (FEA) model is shown in Appendix B. The program used the von Mises yield criterion and kinematic strain hardening with the plastic modulus equal to 2% of the elastic modulus of 29,000 ksi.

A 3.00 in. lateral displacement was applied to the top beam for a 0.025 rad drift angle. Full plastic beam hinges occurred with the hinging region at the ends of the gusset plates. The moment frame action determined by FEA resisted 48% of the frame lateral force at the 0.025 rad drift angle.

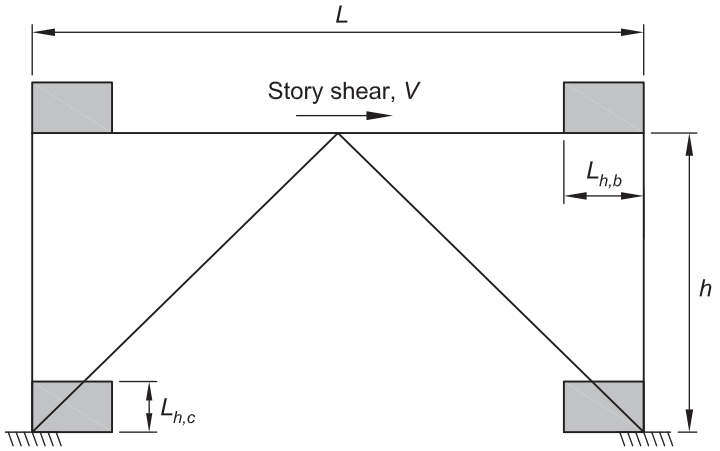

(a) Braced-moment frame

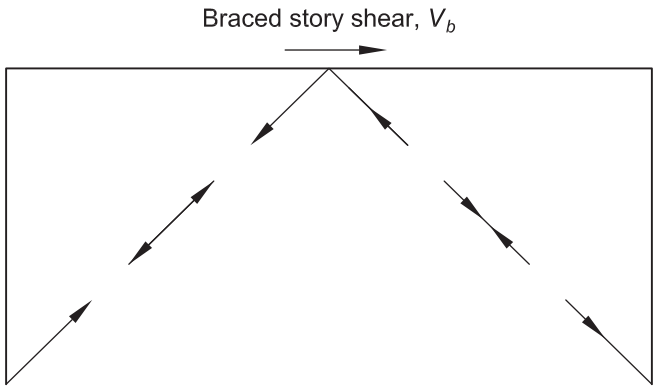

(b) Braced frame

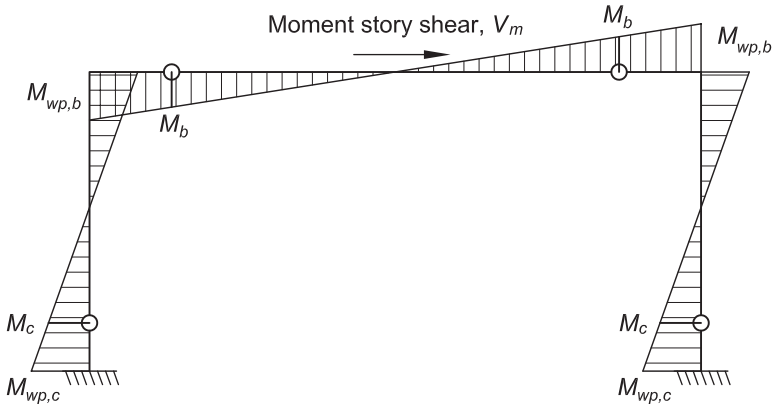

(c) Moment frame force distributions

Fig. 5. Braced-moment frame modeled for analysis of the seismic force distribution as a combination of the force distributions in a braced frame and a moment frame.

For comparative purposes of the beam-moment frame rationale with the FEA results, a lateral force of 1,200 kips was applied at the midpoint of the top beam of the frame shown in Figure 6. The properties of this frame are as follows:

From AISC *Steel Construction Manual* Tables 1-1 and 2-4 (AISC, 2023), the geometric and material properties of the beam and column are as follows:

Beam
W21×101
$A_b = 29.8 \text{ in.}^2$
$Z_{x,b} = 253 \text{ in.}^3$
$d_b = 21.4 \text{ in.}$
$F_y = 54 \text{ ksi (expected)}$

Column
W14×176
$A_c = 51.8 \text{ in.}^2$
$Z_{x,c} = 320 \text{ in.}^3$
$d_c = 15.2 \text{ in.}$
$F_y = 54 \text{ ksi (expected)}$

Frame and gusset geometry:
$L = 240 \text{ in. (working point length of the beam)}$
$h = 120 \text{ in. (working point story height of columns)}$
$L_{p,b} = L_{p,c} = 18 \text{ in. (gusset length/height)}$

The beam axial yield load and pure bending plastic moment are calculated as:

$$P_{y,b} = F_y A_b = (54 \text{ ksi})(29.8 \text{ in.}^2) = 1{,}610 \text{ kips}$$

$$M_{u,b} = F_y Z_{x,b} = (54 \text{ ksi})(253 \text{ in.}^3) = 13{,}700 \text{ kip-in.}$$

The beam hinge length is calculated as the sum of the gusset length and the column halfwidth (i.e., the location of the working point):

$$L_{h,b} = L_p + \frac{d_c}{2} = 18.0 \text{ in.} + \frac{15.2 \text{ in.}}{2} = 25.6 \text{ in.}$$

The beam hinge rotation adjustment factor, $k_{1,b}$, is calculated as:

$$k_{1,b} = 1 + \frac{2L_{h,b}}{L - 2L_{h,b}} \quad \text{(from Eq. A-4)}$$
$$= 1 + \frac{2(25.6 \text{ in.})}{240 \text{ in.} - 2(25.6 \text{ in.})}$$
$$= 1.27$$

The axial load in the beam, P_b, is half the story shear because the columns share the story shear equally. Consequently, k_2 is calculated as:

$$P_b = \frac{V}{2} = \frac{1{,}200 \text{ kips}}{2} = 600 \text{ kips}$$

$$\frac{P_b}{P_{y,b}} = \frac{600 \text{ kips}}{1{,}610 \text{ kips}} = 0.373 > 0.2$$

$$k_{2,b} = \frac{9}{8}\left(1 - \frac{P_b}{P_{y,b}}\right) \quad \text{(from Eq. A-6)}$$
$$= \frac{9}{8}(1 - 0.373)$$
$$= 0.705$$

Using a strain hardening factor of 1.1, the moment capacity of the beam hinge is calculated as:

$$M_b = 1.1 M_u k_{2,b} = 1.1(13{,}700 \text{ kip-in.})(0.705) = 10{,}600 \text{ kip-in.}$$

The moment frame story shear is calculated as:

$$V_m = \frac{4M_b k_{1,b}}{h} = \frac{4(10{,}600 \text{ kip-in.})(1.27)}{120 \text{ in.}} = 449 \text{ kips}$$

This is 37% of the total frame shear of 1,200 kips, which is in agreement with the 48% moment frame action determined by FEA.

The braced frame story shear is calculated as:

$$V_b = V - V_m = 1{,}200 \text{ kips} - 449 \text{ kips} = 751 \text{ kips} \quad (5)$$

This is 63% of the total frame shear of 1,200 kips, which is in agreement with the FEA 52%.

Evaluation of a Lopez Test Frame Using the Column Hinge Mechanism

Shown in Figure 7 are the laboratory test frames designed to evaluate BRBs in braced frames (Lopez et al., 2002, 2004). An analysis for force distributions in the chevron frame is made here.

The properties of the beam and column are as follows:

Beam
W21×93
A_b = 27.3 in.^{2}
$Z_{x,b}$ = 221 in.^{3}
d_b = 21.6 in.
F_y = 54 ksi (expected)

Column
W14×176
A_c = 51.8 in.^{2}
$Z_{x,c}$ = 320 in.^{3}
d_c = 15.2 in.
F_y = 54 ksi (expected)

Frame and gusset geometry:
L = 240 in. (working point length of the beam)
h = 132 in. (working point story height of columns)
$L_{p,b} = L_{p,c}$ = 24 in. (gusset length/height)

The beam axial yield load and pure bending plastic moment are calculated as:

$$P_{y,b} = F_y A_b$$
$$= (54 \text{ ksi})(27.3 \text{ in.}^2)$$
$$= 1{,}470 \text{ kips}$$

$$M_{u,b} = F_y Z_{x,b}$$
$$= (54 \text{ ksi})(221 \text{ in.}^3)$$
$$= 11{,}900 \text{ kip-in.}$$

The beam hinge length is calculated as the sum of the gusset length and the column half width (i.e., the location of the working point):

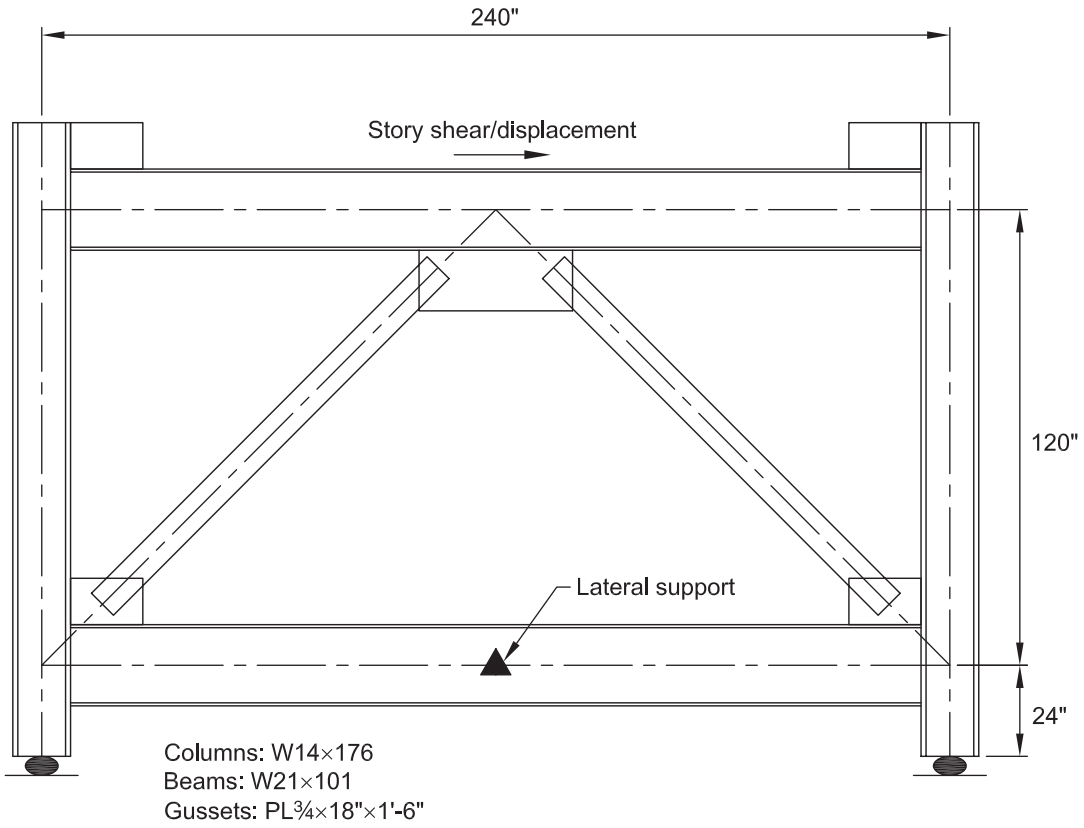

Fig. 6. Single-story chevron test frame.

$$L_{h,b} = L_p + \frac{d_c}{2}$$
$$= 24.0 \text{ in.} + \frac{15.2 \text{ in.}}{2}$$
$$= 31.6 \text{ in.}$$

The beam hinge rotation adjustment factor, $k_{1,b}$, is calculated as:

$$k_{1,b} = 1 + \frac{2L_{h,b}}{L - 2L_{h,b}} \quad \text{(from Eq. A-4)}$$
$$= 1 + \frac{2(31.6 \text{ in.})}{240 \text{ in.} - 2(31.6 \text{ in.})}$$
$$= 1.36$$

The axial load in the beam, P_b, is half the story shear because the columns share the story shear equally. Consequently, k_2 is calculated as:

$$P_b = \frac{V}{2}$$
$$= \frac{1{,}200 \text{ kips}}{2}$$
$$= 600 \text{ kips}$$

$$\frac{P_b}{P_{y,b}} = \frac{600 \text{ kips}}{1{,}470 \text{ kips}}$$
$$= 0.408 > 0.2$$

$$k_{2,b} = \frac{9}{8}\left(1 - \frac{P_b}{P_{y,b}}\right) \quad \text{(from Eq. A-6)}$$
$$= \frac{9}{8}(1 - 0.408)$$
$$= 0.666$$

The column axial yield load and pure bending plastic moment are calculated as:

$$P_{y,c} = F_y A_c$$
$$= (54 \text{ ksi})(51.8 \text{ in.}^2)$$
$$= 2{,}800 \text{ kips}$$

$$M_{u,c} = F_y Z_{x,c}$$
$$= (54 \text{ ksi})(320 \text{ in.}^3)$$
$$= 17{,}300 \text{ kip-in.}$$

The column hinge length is calculated as the gusset height because the working point is at the bottom of the column:

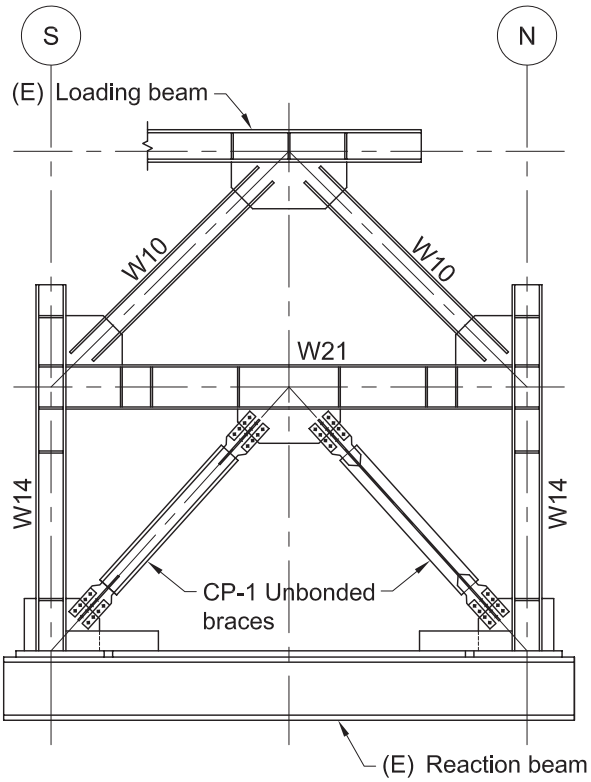

Partial elevation. Setup for test 1.

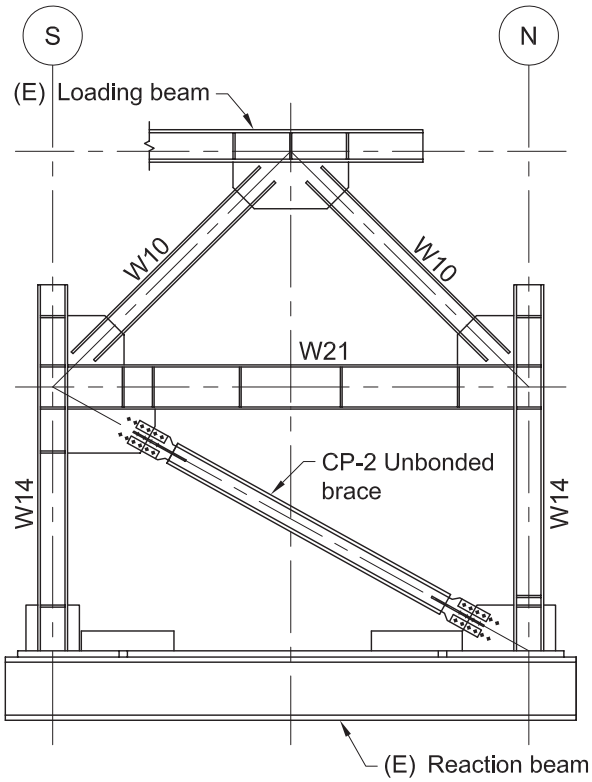

Partial elevation. Setup for tests 2 & 3.

Fig. 7. Laboratory test frames (Lopez et al., 2002, 2004).

$$L_{h,c} = L_{p,c} = 24.0 \text{ in.}$$

The column hinge rotation adjustment factor, $k_{1,c}$, is calculated as:

$$k_{1,c} = 1 + \frac{L_{h,c}}{h - L_{h,c}}$$
$$= 1 + \frac{24.0 \text{ in.}}{132 \text{ in.} - 24.0 \text{ in.}}$$
$$= 1.22$$

The axial load in the column, P_c, is evaluated by equating the frame moment of the axial force to the moment of the shear force [refer to Figure 3 of Lopez et al. (2002), for the frame dimensions]:

$$P_c(240 \text{ in.}) = (1{,}200 \text{ kips})(244 \text{ in.})$$
$$P_c = 1{,}220 \text{ kips}$$

Subsequently, $k_{2,c}$ is calculated as:

$$\frac{P_c}{P_{y,c}} = \frac{1{,}220 \text{ kips}}{2{,}800 \text{ kips}}$$
$$= 0.436 > 0.2$$

$$k_{2,c} = \frac{9}{8}(1 - 0.436)$$
$$= 0.635$$

With two beam plastic hinges, two column plastic hinges, and a strain hardening factor of 1.1, the moment frame shear is:

$$V_m = \frac{1.1(2)}{h}(M_{u,b}k_{1,b}k_{2,b} + M_{u,c}k_{1,c}k_{2,c})$$
$$= \frac{1.1(2)}{132 \text{ in.}}\left[(11{,}900 \text{ kip-in.})(1.36)(0.666) + (17{,}300 \text{ kip-in.})(1.22)(0.635)\right]$$
$$= 403 \text{ kips}$$

This is 34% of the total frame shear of 1,200 kips. This distribution of the shear in this frame is within reasonable agreement with the test results of V_m = 58% [refer to Figures 6 and 9 of Lopez et al. (2002)] in view of the stiffening effects of the frame by the loading truss that was required for testing.

SUMMARY

A rationale is presented herein for buckling-restrained braced frames that includes the inherent moment frame forces when the frame is subjected to seismic forces and displacements. An evaluation of the distribution of the story shear between the braces and the moment frame is made using conventional plastic analysis of the moment frame. This rationale may be used to optimize the story shear distribution to mitigate the effects of the frame distortion forces when the frame is subjected to large seismic and wind loadings. An evaluation of the lateral force distributions in a typical frame by FEA and in the simulated Lopez test frame by the rationale presented herein showed an agreement between the FEA and the laboratory test and analytical model force distributions that supports the rationale presented herein.

REFERENCES

AISC (2022a), *Seismic Provisions for Structural Steel Buildings*, ANSI/AISC 341-22, American Institute of Steel Construction, Chicago, Ill.

AISC (2022b), *Specification for Structural Steel Buildings*, ANSI/AISC 360-22, American Institute of Steel Construction, Chicago, Ill.

AISC (2023), *Steel Construction Manual*, 16th Ed., American Institute of Steel Construction, Chicago, Ill.

ASCE (2022), *Minimum Design Loads and Associated Criteria for Buildings and Other Structures*, ASCE/SEI 7-22, American Society of Civil Engineers, Reston, Va.

ASTM (2020), *Standard Specification for Structural Steel Shapes*, A992/A992M-20, ASTM International, West Conshocken, Pa.

Lopez, W.A., Gwie, D.S., Lauck, T.W., and Saunders, C.M. (2004), "Structural Design and Experimental Verification of a Buckling-Restrained Braced Frame System," *Engineering Journal*, AISC, Vol. 41, No. 4, pp. 177–186.

Lopez, W.A., Gwie, D.S., Saunders, C.M., and Lauck, T.W. (2002), "Lessons Learned from Large-Scale Tests of Unbonded Braced Frame Subassemblies," *Proceedings of the Structural Engineers Association of California 2002 Convention*.

Mahin, S. and Patxi, U. (2002), "Summary of Full Scale Braced Frame Test Using Buckling Restrained Braces," UCB 2002 Test 3, University of California, Berkeley, Calif.

Muir, L.S. and Thornton, W.A. (2014), *Vertical Bracing Connections—Analysis and Design*, Design Guide 29, AISC, Chicago, Ill.

Richard, R.M., Radau, R.E., and Allen, J. (2017), "Damage Tolerant Braced Frame Designs," *Proceedings of the Structural Engineers Association of California 2017 Convention*.

Walters, M.T., Maxwell, B.H., and Berkowitz, R.A. (2002), "Design for Improved Performance of Buckling-Restrained Braced Frames," *Proceedings of the Structural Engineers Association of California 2002 Convention,* pp. 507–513.

APPENDIX A
DERIVATION OF COEFFICIENTS

Derivation of k_1

A braced-moment frame with hinged beams is shown in Figure A-1. Because the hinges are offset from the beam ends, the hinge rotation, θ_h, exceeds the story drift angle, θ, as shown in Figure A-2, where L is the beam length.

The hinge rotation is calculated as:

$$\begin{aligned}\theta_h &= \theta + \frac{2\theta L_h}{L - 2L_h} \\ &= \theta\left(1 + \frac{2L_h}{L - 2L_h}\right) \\ &= \theta k_1\end{aligned} \tag{A-1}$$

where

$$\begin{aligned}k_1 &= 1 + \frac{2L_h}{L - 2L_h} \\ &= \frac{L}{L - 2L_h}\end{aligned} \tag{A-2}$$

A generalized braced frame (i.e., chevron or diagonal) may have moment hinge lengths, $L_{h,a}$ and $L_{h,b}$, that differ on either side of the member. For this case, k_1 differs on each side of the member and is calculated separately for each side as:

$$\begin{aligned}k_{1,a} &= 1 + \frac{2L_{h,a}}{L - L_{h,a} - L_{h,b}} \\ &= \frac{L + L_{h,a} - L_{h,b}}{L - L_{h,a} - L_{h,b}}\end{aligned} \tag{A-3}$$

$$\begin{aligned}k_{1,b} &= 1 + \frac{2L_{h,b}}{L - L_{h,a} - L_{h,b}} \\ &= \frac{L - L_{h,a} + L_{h,b}}{L - L_{h,a} - L_{h,b}}\end{aligned} \tag{A-4}$$

The member shear is calculated by adding the working point moments, which only differ by the factors $k_{1,a}$ and $k_{1,b}$, and dividing by the member length. An effective k_1 factor can be calculated as:

$$\begin{aligned}k_1 &= \frac{k_{1,a} + k_{1,b}}{2} \\ &= \frac{L}{L - L_{h,a} - L_{h,b}}\end{aligned} \tag{A-5}$$

This formulation can be used for all frame calculations when member hinge locations relative to the working points are known. Note that for the symmetric case where $L_{h,a} = L_{h,b} = L_h$, k_1 simplifies to the general case. When only one hinge exists on a member, as with columns in the column mechanism, setting one hinge length to zero provides an accurate yet conservative result for the moment frame proportion of the base shear.

Derivation of k_2

The beam plastic moment capacity, M_p, is evaluated using beam-column interaction equations given in AISC *Specification* Section H1 (AISC, 2022b). Assuming the beams (with gross area, A_b, and strong-axis plastic modulus, Z_x) are in uniaxial bending, the moment capacity for a given axial load, P, is found by rearranging the equations:

$$k_2 = \frac{M_p}{M_u} = \begin{cases} \dfrac{9}{8}\left(1 - \dfrac{P}{P_y}\right), \text{ for } \dfrac{P}{P_y} \geq 0.2 \\ 1 - \dfrac{P}{2P_y}, \text{ for } \dfrac{P}{P_y} < 0.2 \end{cases} \tag{A-6}$$

where

$$P_y = F_y A_b \tag{A-7}$$

$$M_u = F_y Z_x \tag{A-8}$$

APPENDIX B
FINITE ELEMENT ANALYSIS RESULTS

Shown in Figure B-1 is the FEA model used to analyze the Figure 6 truss. Beams, columns, braces, and plates were modeled using 20-node hexahedrons. Fillet welds were modeled using 10-node tetrahedrons. The BRB core area yield stress was 42 ksi. This FEA model comprised approximately 468,000 nodes and 96,000 elements (Richard et al., 2017).

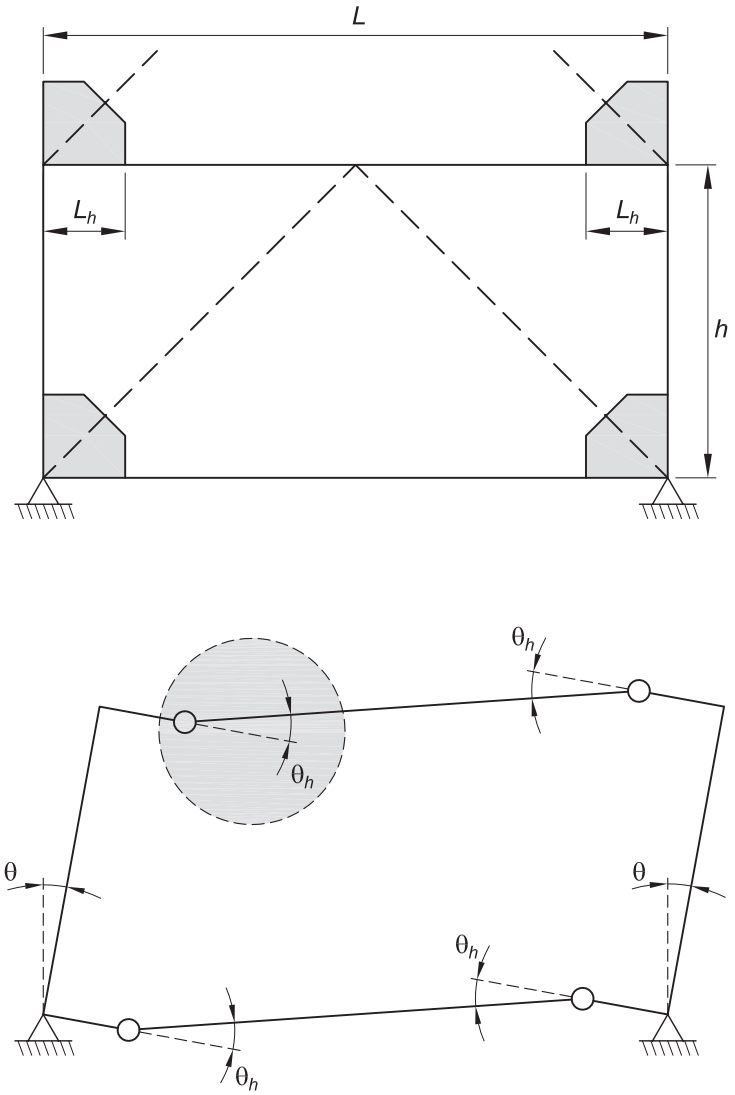

Fig. A-1. Moment frame story geometry and plastic hinge mechanism.

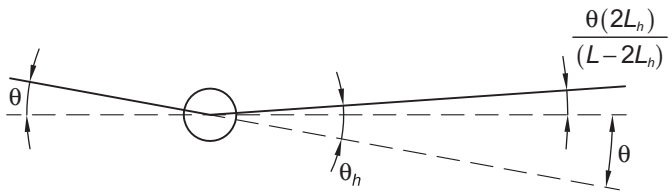

Fig. A-2. Magnified view of plastic hinge rotation from Figure A-1.

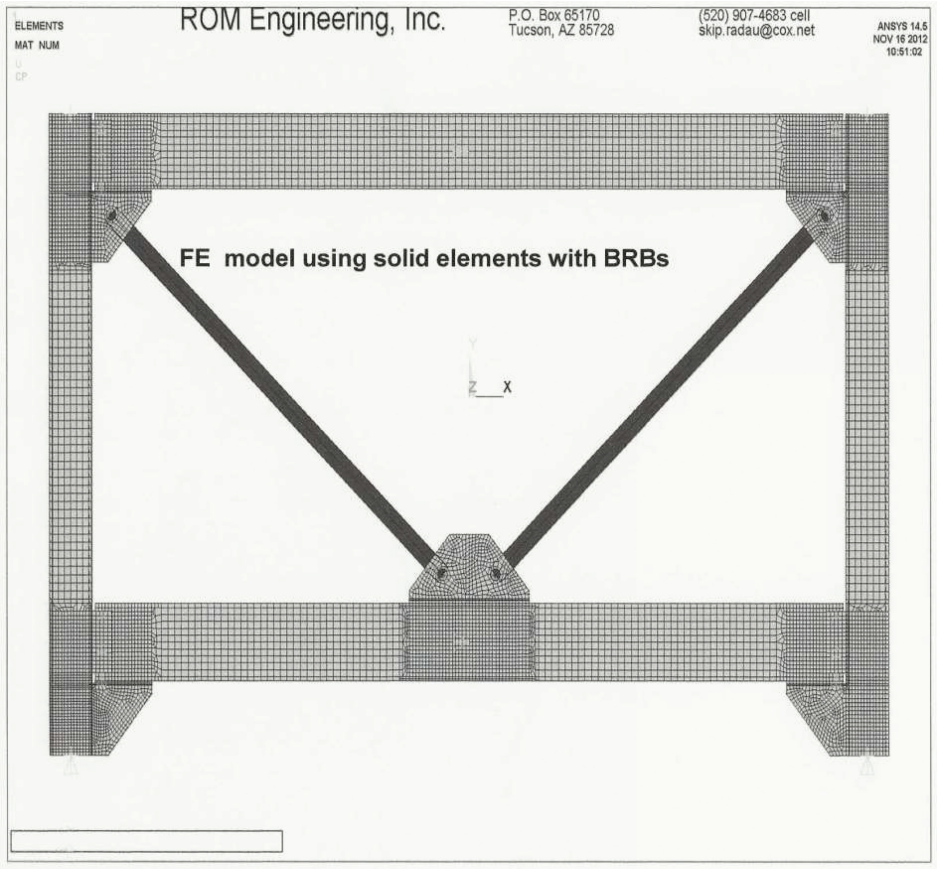

Fig. B-1. Finite element model of the frame shown in Figure 6.

The Adoption of AISC 360 for Offshore Structural Design Practices

ALBERT KU, FARREL ZWERNEMAN, STEVE GUNZELMAN, and JIEYAN CHEN

ABSTRACT

The offshore design standards for U.S. practices refer to AISC specifications when designing structural components with nontubular shapes. The widely used API RP-2A WSD standard (API, 2014) asks designers to use the 1989 AISC *Specification* (AISC, 1989a). The newly published API RP-2A LRFD (API, 2019) and RP-2TOP (ANSI/API, 2019) ask designers to use the 2010 AISC *Specification* (AISC, 2010). Although the 2010 AISC *Specification* has been partially adopted by API, the current offshore practice is still primarily dominated by the 1989 AISC *Specification*. The key issue hampering the offshore community's full adoption of the 2010 AISC *Specification* is the relative ease of accounting for second-order effects in the 1989 AISC *Specification*. In 2019, API formed a Task Group dedicated to studying this issue, with the main findings summarized in this paper. By illustrating the key code check process in two examples with an easy-to-understand format, this paper aims at assisting the offshore structural engineers to better understand the latest AISC *Specification*. The authors also hope that this paper will serve as a communication path between the offshore structural community and AISC for current and future standards' adoption and harmonization.

Keywords: offshore structural design, topsides structural design, API RP-2A, API RP-2TOP.

INTRODUCTION

For the offshore industry, use of the 1989 AISC *Specification for Structural Steel Buildings* (AISC, 1989a) together with the 9th Edition *Steel Construction Manual* (AISC, 1989b) has been a long-held tradition. When the American Petroleum Institute (API) issued the most recent working stress design (WSD) standard—the API RP-2A WSD, 22nd Edition (API, 2014), in 2014—use of the AISC *Specification for Structural Steel Buildings*, ANSI/AISC 360, hereafter referred to as AISC 360, was explicitly discouraged in both the Foreword and Section 6.1.1 of that API document. The fundamental reason for API's hesitation to adopt AISC 360 has been a lack of sufficient understanding on the new frame stability provisions, and its associated second-order analysis concept. It is our hope that this paper will benefit other offshore structural engineers who wish to understand the issues of transitioning from the 1989 AISC *Specification* to AISC 360-16 (AISC, 2016).

Albert Ku, PhD, PE, Principal Engineer, DNV Energy Systems, New Taipei City, Taiwan. Email: albert.ku@dnv.com (corresponding)

Farrel Zwerneman, Independent Consultant, Houston, Tex. Email: fzwern0@gmail.com

Steve Gunzelman, Independent Consultant, Houston, Tex. Email: gunzclan@earthlink.net

Jieyan Chen, Structural Engineer, IntelliSIMS, Houston, Tex. Email: jieyan@intellisims.com

Paper No. 2023-04

On AISC's frame stability procedure, excellent references can be found in AISC Design Guide 28, *Stability Design of Steel Buildings* (Griffis and White, 2013), the summary paper by Carter and Geschwindner (2008), the summary note by Carter (2013), and the SSRC *Stability Guide* (Ziemian, 2010). The lead author of this paper found Carter and Geschwindner (2008) to be particularly lucid and benefited with a good understanding of the AISC 360 frame stability process after reading that work. In this paper, we attempt to follow the same style by giving simple examples with clear explanations on the calculation process. In addition, the comparison paper between the AISC *Specification* and Eurocode 3 by Bernuzzi et. al. (2015) is also of note.

It should be noted that API did adopt a version of AISC 360 [AISC 360-10, which corresponds to the 14th Edition *Manual* (AISC, 2011)] in 2019 with the publication of API RP-2TOP (ANSI/API, 2019). The 2016 AISC *Specification*, AISC 360-16, was not adopted because the 2TOP draft was prepared before 2016. Although the API RP-2TOP document adopts AISC 360-10, this AISC *Specification* and its associated frame stability concept are still foreign to most offshore structural engineers. Its relation to tubular structural designs, which form the core of API RP-2A WSD and RP-2A LRFD, are also not well understood.

The first offshore platform was installed in 1948 in the Gulf of Mexico. In the early years of offshore oil and gas platform design, construction, and installation, there were no specific standards applicable to this industry. Offshore structural engineers had to rely on onshore steel structure experiences and the standards as published by AISC. The 1st Edition API RP-2A design standard, *API Recommended*

Practice for Planning, Designing, and Constructing Fixed Offshore Platforms, was published in 1969 with 16 pages (API, 1969). In the span of 45 years (1969–2014), there would be 21 more editions of API RP-2A based on the working stress design (WSD) concept, with the latest, API RP-2A WSD 22nd Edition (2014), expanded to 310 pages. Throughout these editions, the connection to AISC *Specifications* has been important. The connection lies in the adopted equations (for tubular member design use) and its explicit requirement to use AISC *Specifications* for non-tubular member designs.

API published its first LRFD-based RP-2A in 1993 (API, 1993), and in this standard, the connection to the 1986 AISC LRFD *Specification* (AISC, 1986) was referenced. However, the use of this LRFD standard had been very limited in the United States, and the offshore industry continued to be dominated by the WSD design practice. API retracted the 1st Edition API 2A-LRFD in 2012 due to a lack of technical maintenance. This standard was upgraded and reissued in 2019 as the API RP-2A LRFD 2nd Edition (API, 2019). Whether the use of this new LRFD standard will be more widespread remains to be seen.

Fixed offshore structures are typically completely braced, as shown on the left side of Figure 1. In some geographical areas with low seismicity, such as the Gulf of Mexico, many jackets have a "portal bay" in between the jacket and topsides (i.e., deck) as shown on the right side of Figure 1. This can be due to installation requirements or a desire to reduce the wave load in the splash zone. This portal bay will experience the second-order effect (P-Δ effect) the most, when compared to other braced parts of the structure. In addition, equipment support modules on the topsides can be unbraced. Designers for these two types of structure—namely, the jacket portal bay and the unbraced equipment support module—should be keenly aware of the latest AISC standard requirement related to frame stability.

From the authors' point of view, the differences between the AISC 1989 *Specification* and AISC 360-16 are primarily in the beam-column code check, and the types of structural analysis required for that check. This is summarized in Table 1. For code checks using the 1989 *Specification*, the structural analysis should be first-order based. The beam-column equation in the 1989 *Specification* contains a magnification factor on the bending stress to represent the second-order effect.

For code checks using AISC 360-16, the structural analysis should be second-order based. Because the structural load demands obtained from the analyses already include the second-order effect, the beam-column equations no longer require a magnification factor.

In AISC 360-16, three types of frame stability analysis can be employed: the effective-length method (ELM), the direct-analysis method (DM), and the first-order method (FOM). A summary is shown in Table 2. The detailed discussions on these methods will be postponed until the examples are presented.

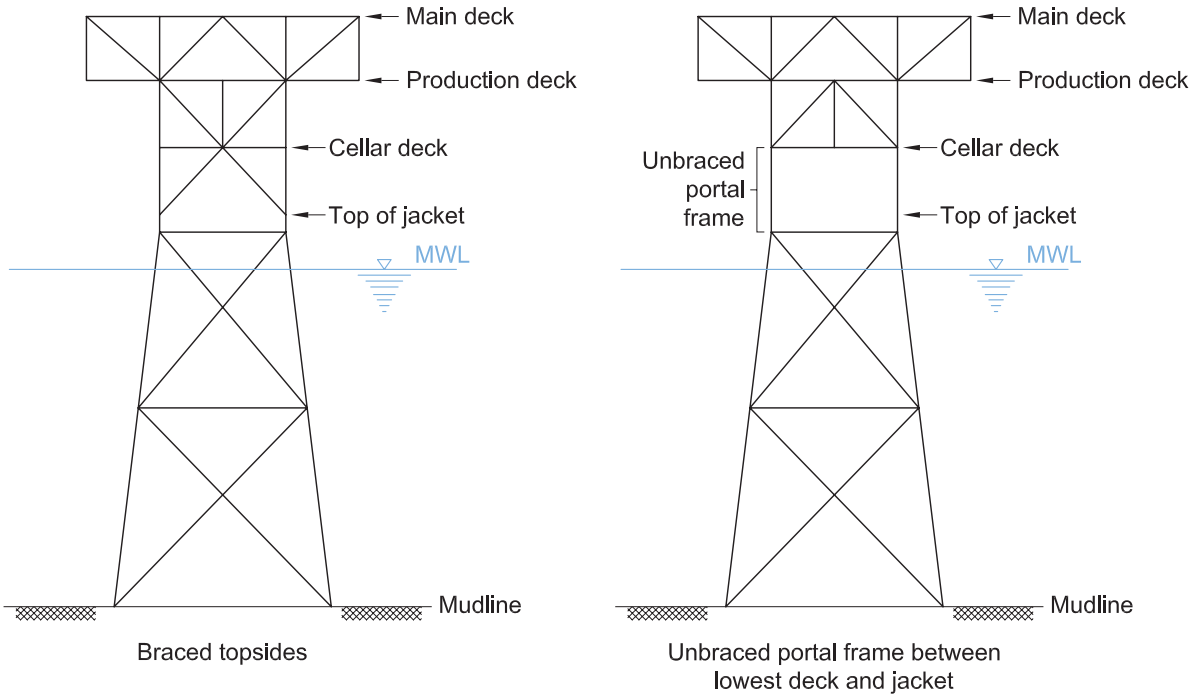

Fig. 1. Braced offshore structure (left) and partially braced with portal bay (right).

Table 1. Summary of the Beam-Column Check for the AISC 1989 and 2016 *Specifications*		
	AISC 1989 *Specification*	**AISC 2016 *Specification***
Structural analysis method	First-order based	Second-order based
Beam-column unity check equation	$\frac{f_a}{F_a}+\frac{C_{mx}f_{bx}}{\left(1-\frac{f_a}{F'_{ex}}\right)F_{bx}}+\frac{C_{my}f_{by}}{\left(1-\frac{f_a}{F'_{ey}}\right)F_{by}}\le 1.0^{(1)}$ Second-order magnified	$\frac{P_r}{P_c}+\frac{8}{9}\left(\frac{M_{rx}}{M_{cx}}+\frac{M_{ry}}{M_{cy}}\right)\le 1.0^{(2)}$ No magnification
Notes: (1): Only the buckling equation is shown (2): For the $P_r/P_c > 0.2$ segment		

In this paper, two examples are considered: a cantilever beam-column and a two-dimensional structure with a portal bay. In the cantilever example, two levels of horizontal load are examined. Offshore structures are subjected to lateral loads from wind, wave, and current, and they are checked in combination with gravity loads. A lateral-to-vertical load ratio of 2% is on the low side; the more typical ratio will be 5% or higher. A structural member designed to the 5% lateral-to-vertical ratio will have a higher bending code check component (and lower axial component) than the 2% lateral-to-vertical case. Since the second-order effect is strongly associated with the P-Δ effect, the 5% case with the lower axial load will have a lower second-order effect. This will reflect on their B_2 values to be discussed later.

In the cantilever example, unity code check values for the 2% and 5% lateral-to-vertical load ratios are both examined. Although 5% is the more typical case for offshore structures, in the 2D structure example, only the 2% case will be given. This is due to the paper's length limit, as well as that the 2% case will generate higher second-order effects. Consequently, these results are more interesting for frame stability considerations. The code checks performed in this paper are ASD or WSD checks with no additional allowable stress increase. The cases examined are summarized in Table 3.

CAPACITY EQUATIONS

Capacity equations can be found in the AISC *Specification*, Section E for compression, Section F for flexure, and Section H for beam-columns. In this section of the paper, only the general forms of these equations are listed for the purpose of explaining code check procedures. Refer to AISC 360-16 (AISC, 2016) and the 1989 AISC *Specification* (1989a), for equation details and associated notations. In the following, the equation numbers from the original references are also listed.

AISC 1989 *Specification*

The beam-column checks must satisfy the following two equations, with the first equation related to buckling and the second equation related to yielding. Both equations need to be satisfied.

$$\frac{f_a}{F_a}+\frac{C_{mx}f_{bx}}{\left(1-\frac{f_a}{F'_{ex}}\right)F_{bx}}+\frac{C_{my}f_{by}}{\left(1-\frac{f_a}{F'_{ey}}\right)F_{by}}\le 1.0 \quad (1)$$

Spec. Eq. H1-1

$$\frac{f_a}{0.6F_y}+\frac{f_{bx}}{F_{bx}}+\frac{f_{by}}{F_{by}}\le 1.0 \quad (2)$$

Spec. Eq. H1-2

The allowable axial compression stress is:

$$F_a=\begin{cases}\dfrac{\left[1-\dfrac{(KL/r)^2}{2C_c^2}\right]F_y}{\dfrac{5}{3}+\dfrac{3(KL/r)}{8C_c}-\dfrac{(KL/r)^3}{8C_c^3}}, & \dfrac{(KL/r)}{C_c}\le 1.0 \\ \dfrac{12\pi^2E}{23(KL/r)^2}, & \dfrac{(KL/r)}{C_c}>1.0\end{cases} \quad (3)$$

Spec. Eq. E2-1

Spec. Eq. E2-2

The allowable bending stress of I-shaped members is:

$$F_b=0.66F_y \qquad L_b\le L_c \quad (4)$$

Spec. Eq. F1-1

L_c is given by:

$$L_c=\min\left\{\frac{76b_f}{\sqrt{F_y}},\ \frac{20{,}000}{(d/A_f)F_y}\right\} \quad (5)$$

Spec. Eq. F1-2

When the unbraced length is greater than L_c, the allowable bending stress is:

Table 2. Summary of ELM, DM, and FOM			
	Effective-Length Method (ELM)	**Direct-Analysis Method (DM)**	**First-Order Method (FOM)**
Limitation	$B_2 = \frac{\Delta_{2nd}}{\Delta_{1st}} \le 1.5$ (Δ = average story drift)	None[1]	$B_2 \le 1.5$, $\frac{\alpha P_r}{P_y} \le 0.5$
Analysis type	Second-order elastic	Second-order elastic	First-order elastic
Notional lateral loads[4]	$N_i = 0.002Y_i$, minimum[3] (Y_i = gravity load applied at level i, LRFD or 1.6 times the ASD load combinations)	$N_i = 0.002Y_i$ (minimum lateral load if $B_2 \le 1.5$; additive if $B_2 > 1.5$)	$N_i = 2.1\left(\frac{\Delta}{L}\right)Yi \ge 0.0042\left(\frac{Y_i}{\alpha}\right)$ additive[3]
Member stiffness	Nominal EA, EI	Reduced $EA^* = 0.8\tau_b EA$, $EI^* = 0.8EI$ τ_b[2] $= \begin{cases} 1.0 \text{ when } \alpha P_r/P_y \le 0.5 \\ 4(\alpha P_r/P_y)\left[1-(\alpha P_r/P_y)\right] \end{cases}$[5]	Nominal EA, EI
K factor	Buckling analysis from API/AISC guidance	$K = 1.0$	$K = 1.0$

Notes: (1) Though DM can apply to high B_2, it is recommended to limit $B_2 \le 1.5$ for offshore design as a rule.

(2) In DM, EA and EI are reduced by 20% to represent cross-sectional premature yielding due to residual stress. If axial load is high ($\alpha P_r/P_y > 0.5$), cross-sectional stiffness is further reduced by τ_b.

(3) Minimum: if actual applied loads are greater, N_i is ignored. Additive: N_i is applied regardless of actual lateral load.

(4) Notional lateral loads for ELM and DM are meant to represent initial out-of-plumbness. Notional lateral loads for FOM are meant to represent second-order load effect with a first-order structural analysis.

(5) τ_b can be taken as 1.0 in all members if additional notional loads of $0.001Y_i$ are applied to lateral loads.

Table 3. Code Check Cases Performed in This Study		
	Cantilever	**2D Jacket**
H* = 5%*P		
AISC 1989 *Specification*	√	—
AISC 360-16 ELM	√	—
AISC 360-16 DM	—	—
AISC 360-16 FOM	—	—
H* = 2%*P		
AISC 1989 *Specification*	√	√
AISC 360-16 ELM	√	√
AISC 360-16 DM	—	√
AISC 360-16 FOM	—	√

$$F_b = \begin{cases} \left[\frac{2}{3} - \frac{F_y (L_b/r_T)^2}{1530\times10^3 C_b}\right] F_y \le 0.60F_y, \\ \sqrt{\frac{102\times10^3 C_b}{F_y}} \le \frac{L_b}{r_T} \le \sqrt{\frac{510\times10^3 C_b}{F_y}} \\ \frac{170\times10^3 C_b}{(L_b/r_T)^2} \le 0.60F_y, \quad \frac{L_b}{r_T} > \sqrt{\frac{510\times10^3 C_b}{F_y}} \end{cases} \quad (6)$$

Spec. Eq. F1-6
Spec. Eq. F1-7

AISC 360-16

Beam-column checks must satisfy the following two equations. These two equations are in fact one equation but with different slopes on the *P-M* interaction diagram:

$$\frac{P_r}{P_c} + \frac{8}{9}\left(\frac{M_{rx}}{M_{cx}} + \frac{M_{ry}}{M_{cy}}\right) \le 1.0, \quad \frac{P_r}{P_c} \ge 0.2 \quad (7)$$

Spec. Eq. H1-1a

$$\frac{P_r}{2P_c} + \left(\frac{M_{rx}}{M_{cx}} + \frac{M_{ry}}{M_{cy}}\right) \le 1.0, \quad \frac{P_r}{P_c} < 0.2 \quad (8)$$

Spec. Eq. H1-1b

The nominal axial strength is as follows:

$$P_n = F_{cr} A_g \quad (9)$$

Spec. Eq. E3-1

$$F_{cr} = \begin{cases} \left(0.658^{\frac{F_y}{F_e}}\right) F_y, & \frac{F_y}{F_e} \le 2.25 \\ 0.877F_y, & \frac{F_y}{F_e} > 2.25 \end{cases} \quad (10)$$

Spec. Eq. E3-2
Spec. Eq. E3-3

The nominal flexural strength is as follows:

$$M_n = \begin{cases} M_p = F_y Z_x, \quad L_b \le L_p \\ C_b\left[M_p - (M_p - 0.75F_y S_x)\left(\frac{L_b - L_p}{L_r - L_p}\right)\right] \le M_p, \\ \qquad L_p < L_b \le L_r \\ F_{cr} S_x \le M_p, \quad L_b > L_r \end{cases} \quad (11)$$

Spec. Eq. F2-1
Spec. Eq. F2-2
Spec. Eq. F2-3

$$F_{cr} = \frac{C_b \pi^2 E}{(L_b/r_{ts})^2}\sqrt{1 + 0.078\frac{Jc}{S_x h_0}\left(\frac{L_b}{r_{ts}}\right)^2} \quad (12)$$

Spec. Eq. F2-4

API RP-2A WSD (2014) Tubular Capacity Equations

In the second code check example, the 2D portal frame jacket, the tubular portal frame columns will be checked using the stability methods listed in Table 2, with the tubular capacity equations taken from API. The tubular beam-column interaction equations are given by API RP-2A WSD as:

$$\frac{f_a}{F_a} + \frac{C_m\sqrt{f_{bx}^2 + f_{by}^2}}{\left(1 - \frac{f_a}{F_e'}\right)F_b} \le 1.0 \quad (13)$$

6.20

$$\frac{f_a}{0.6F_y} + \frac{\sqrt{f_{bx}^2 + f_{by}^2}}{F_b} \le 1.0 \quad (14)$$

6.21

The axial allowable stress is identical to Equation 3. The tubular flexural allowable stress is as follows:

$$F_b, \text{ksi} = \begin{cases} 0.75F_y, & \frac{D}{t} \le \frac{1{,}500}{F_y} \\ \left(0.84 - 1.74\frac{F_y D}{Et}\right)F_y, & \frac{1{,}500}{F_y} < \frac{D}{t} \le \frac{3{,}000}{F_y} \\ \left(0.72 - 0.58\frac{F_y D}{Et}\right)F_y, & \frac{3{,}000}{F_y} < \frac{D}{t} \le 300 \end{cases} \quad (15)$$

6.6
6.7
6.8

where D is the outer diameter and t is the thickness of the tube. The similarities of beam-column interaction and axial allowable stress between the API RP-2A WSD and the 1989 AISC *Specification* indicate that the API equations and its frame stability method were formulated based on the 1989 *Specification* or prior.

DESIGN EXAMPLE 1

Given:

Perform the code checks for a cantilever W14×82 column 15 ft in length. Minor-axis column buckling is fully braced, with the code check performed in the major-axis direction. Use $K = 2.0$, $C_b = 1.67$, and $C_m = 0.85$. The loading is as follows:

$P = 300$ kips ($\beta = 2\%$)

$P = 210$ kips ($\beta = 5\%$)

Solution:

The geometric and material properties of the column are:

W14×82
$A_g = 24.0$ in.^{2}
$I_x = 881$ in.^{4}
$S_x = 123$ in.^{3}
$r_x = 6.06$ in.
$E = 29{,}000$ ksi

The cantilever is schematically shown in Figure 2. The first-order moment, the second-order P-Δ moment, and the second-order P-δ moment are illustrated in the same figure for the $H = 2\%P$ case. Note that the moments as shown have been magnified by the α factor. The purpose of this factor will be discussed in the following.

Load and Deflection Analyses

First-Order Load and Deflection

The first-order moment at the cantilever base is the top horizontal load multiplied by the height of the cantilever, $M_r = (\beta P)L$.

For the $H = 5\%P$ case,

$$M_r = 5\%(210 \text{ kips})(15 \text{ ft})$$
$$= 158 \text{ kip-ft}$$

For the $H = 2\%P$ case,

$$M_r = 2\%(300 \text{ kips})(15 \text{ ft})$$
$$= 90 \text{ kip-ft}$$

The selection of the axial loads, P, for these two cases is such that the unity checks result in approximately 0.90 for both cases.

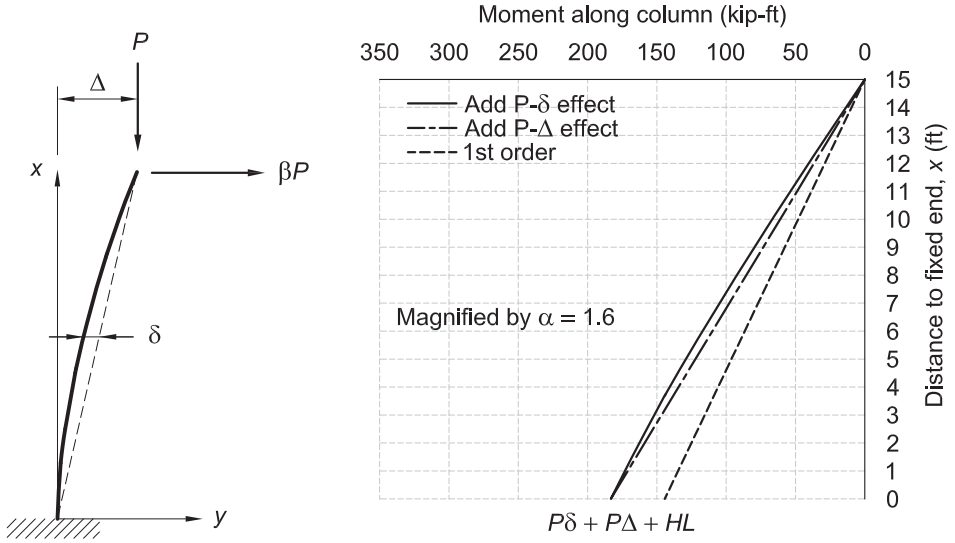

Fig. 2. Cantilever and moment distribution along member length.

The cantilever top deflection, for the case of $H = 2\%P$, can be calculated as:

$$\Delta_{1st} = \frac{\alpha(\beta P)L^3}{3EI}$$
$$= \frac{1.6(0.02)(300 \text{ kips})(15 \text{ ft})^3}{3(29{,}000 \text{ ksi})(881 \text{ in.}^4)}$$
$$= 0.731 \text{ in.}$$

Note that an α factor of 1.6 was used in the deflection calculation. This is due to the requirement that the second-order effect needs to be assessed under the "factored" load. If LRFD is considered, $\alpha = 1.0$; $\alpha = 1.6$ for ASD or WSD. The deflection of 0.731 in., although a first-order value, will be used to assess the second-order effect.

Second-Order Load and Deflection

Geometric nonlinear beam-column analysis provides the second-order deflection along the cantilever height (see McGuire et. al., 2014):

$$y(x) = \frac{\beta}{\sqrt{\frac{\alpha P}{EI}}\cos\left(\sqrt{\frac{\alpha P}{EI}}L\right)}\sin\left(\sqrt{\frac{\alpha P}{EI}}x\right) - \beta x \tag{16}$$

The cantilever top deflection, for the case of $H = 2\%P$, is:

$$\sqrt{\frac{\alpha P}{EI}} = \sqrt{\frac{1.6(300 \text{ kips})}{(29{,}000 \text{ ksi})(881 \text{ in.}^4)}}$$
$$= 4.33\times10^{-3} \text{ in.}^{-1}$$

$$\Delta_{2nd} = 2\%\frac{\sin\left[(4.33\times10^{-3} \text{ in.}^{-1})(15 \text{ ft})\right]}{(4.33\times10^{-3} \text{ in.}^{-1})\cos\left[(4.33\times10^{-3} \text{ in.}^{-1})(15 \text{ ft})\right]} - 2\%(15 \text{ ft})$$
$$= 0.967 \text{ in.}$$

Because the second-order base moment is the combination of $\beta(\alpha P)L + (\alpha P)\Delta_{2nd}$, this moment is calculated to be:

$$M_r = \frac{(0.02)(1.6)(300 \text{ kips})(15\text{ft}) + (1.6)(300 \text{ kips})(0.967 \text{ in.})}{1.6}$$
$$= 114 \text{ kip-ft}$$

Note that the deflection and second-order effect are assessed at the αP level. The load and/or moment are first calculated under this factored condition, and then divided by α for code checks.

The parameter B_2 is an important indicator of the intensity of the second-order effect. This has been implied in Table 2, in which $B_2 = 1.5$ is used as a validity threshold on many of the frame stability calculation methods. B_2 is defined as the ratio between second- to first-order frame deflections. Hence, for the case of $H = 2\%P$, the B_2 factor is:

$$B_2 = \frac{\Delta_{2nd}}{\Delta_{1st}}$$
$$= \frac{0.967 \text{ in.}}{0.731 \text{ in.}}$$
$$= 1.32$$

In lieu of performing a second-order structural analysis, AISC provides an approximate estimate of B_2 that requires only a first-order structural analysis. This approximate formula is:

$$B_2 = \frac{1}{1 - \frac{\alpha P_{story}}{P_{e\,story}}} \tag{17}$$

where $P_{e\ story}$ is the estimate of story elastic critical buckling strength, expressed as:

$$\begin{aligned} P_{e\,story} &= R_m \frac{HL}{\Delta_{1st}} \\ &= 0.85\left[\frac{1.6(2\%)(300\text{ kips})(15\text{ ft})}{(0.731\text{ in.})}\right] \\ &= 2{,}010\text{ kips} \end{aligned}$$

This is compared to the classical Euler buckling load for the cantilever:

$$\begin{aligned} P_{cr} &= \frac{\pi^2 EI}{(KL)^2} \\ &= \frac{\pi^2(29{,}000\text{ ksi})(881\text{ in.}^4)}{\left[2.0(15\text{ ft})\right]^2} \\ &= 1{,}950\text{ kips} \end{aligned}$$

This indicates that $P_{e\ story}$ is a good approximation of P_{cr}. $P_{e\ story}$ applies to frames with more complex geometries other than cantilevers. It should be noted that $P_{e\ story}$ is a floor buckling concept—that is, when a floor with multiple columns reaches its buckling capacity. When assessing frame stability, $P_{e\ story}$ is more relevant as a capacity indicator than the individual column P_{cr}.

Substituting $P_{e\ story}$ into Equation 17,

$$\begin{aligned} B_2 &= \frac{1}{1 - \frac{1.6(300\text{ kips})}{(2{,}010\text{ kips})}} \\ &= 1.31 \end{aligned}$$

This is compared to the analytical B_2 of 1.32 calculated previously based on the deflection definition, and again this shows good agreement. AISC 360-16, Appendix 8, also provides an approximation to the second-order loads as follows:

$$\begin{aligned} P_r &= P_{nt} + B_2 P_{lt} \\ M_r &= B_1 M_{nt} + B_2 M_{lt} \end{aligned} \tag{18}$$

P_{nt} and M_{nt} are the member axial load and moment under only the vertical load, in which the subscript *nt* stands for "no-translation." P_{lt} and M_{lt} are the member axial load and moment under only the horizontal load, in which the subscript *lt* stands for "lateral-translation." P_{nt}, M_{nt}, P_{lt}, and M_{lt} are all obtained from the first-order analysis.

$$\begin{aligned} P_r &= P_{nt} + B_2 P_{lt} \\ &= (300\text{ kips}) + 1.31(0\text{ kips}) \\ &= 300\text{ kips} \end{aligned}$$

$$\begin{aligned} M_r &= B_1 M_{nt} + B_2 M_{lt} \\ &= B_1(0\text{ kip-ft}) + 1.31(0.02)(300\text{ kips})(15\text{ ft}) \\ &= 118\text{ kip-ft} \end{aligned}$$

Table 4. First- and Second-Order Loads for the Cantilever Example			
	P_r (kips)	M_r (kips-ft)	B_2
H* = 5%*P			
First order	210	158	—
Second order	210	185	1.21
H* = 2%*P			
First order	300	90	—
Second order	300	114	1.32

These are compared to the second-order analytical results of $P_r = 300$ kips and $M_r = 114$ kip-ft from the previous calculations based on actual loads. This close agreement demonstrates the usefulness of the $B_1 - B_2$ method.

Designers have the choice of using structural software to automatically calculate the second-order responses. The designer can also opt for obtaining the first-order responses first and then applying the $B_1 - B_2$ method. This $B_1 - B_2$ method is quite versatile and applies to structures with more complex geometries than a simple cantilever. However, for offshore structures with several open frames (e.g., portal frame plus several unbraced topsides module-support structures), it may be difficult to efficiently perform the $B_1 - B_2$ analysis method.

Even if the designers choose to perform a full second-order computer analysis, it is important for them to be aware of this simplified $B_1 - B_2$ method in order to check their computer results. The first- and second-order loads required for further cantilever code checks are summarized in Table 4.

Case of *H* = 5%*P*

***Code Check Using the 1989 AISC* Specification**

The following load demands at the cantilever base are taken from Table 4. Referring to Table 1, it is noted that the first-order loads need to be used with the 1989 *Specification* check.

$P_r = 210$ kips

$M_r = 158$ kip-ft

The applied axial and bending stresses are then as follows:

$$f_a = \frac{P_r}{A_g} = \frac{210 \text{ kips}}{24 \text{ in.}^2} = 8.75 \text{ ksi}$$

$$f_b = \frac{M_r}{S_x} = \frac{158 \text{ kip-ft}}{123 \text{ in.}^2} = 15.3 \text{ ksi}$$

The allowable axial and bending stresses are calculated using Equations 3, 4, and 6. The AISC *Steel Construction Manual* (2017) provides many convenient charts and tables where these capacities can be efficiently evaluated. Hence, we will not provide the calculation details. The capacity values are directly provided here:

$F_a = 22.8$ ksi

$F_b = 30$ ksi

The following factored Euler buckling stress is also required for code checks:

$$F_e' = \frac{12\pi^2 E}{23(KL/r)^2}$$
$$= \frac{12\pi^2 (29{,}000 \text{ ksi})}{23\left[(2.0)(15 \text{ ft})/(6.06 \text{ in.})\right]^2}$$
$$= 42.3 \text{ ksi}$$

The 1989 *Specification* unity check value is thus calculated as:

$$\frac{f_a}{F_a} + \frac{C_m f_b}{\left(1 - \frac{f_a}{F_e'}\right)F_b} = \frac{8.75 \text{ ksi}}{22.8 \text{ ksi}} + \frac{0.85(15.4 \text{ ksi})}{\left(1 - \frac{8.75 \text{ ksi}}{42.3 \text{ ksi}}\right)(30 \text{ ksi})}$$
$$= 0.932$$

Code Check Using the AISC 360-16 ELM

The load demands at the base of the cantilever are taken from Table 4. Note that the second-order loads need to be used with AISC 360-16.

$P_r = 210$ kips
$M_r = 185$ kip-ft

The nominal axial and flexural strengths are calculated, based on Equations 9 and 11, to be $P_n = 927$ kips and $M_n = 579$ kip-ft. As mentioned earlier, standard charts and tables exist for fast capacity calculations; thus their details are not provided here. To be used for ASD, these nominal strengths are reduced by the ASD safety factor, Ω_c:

$$P_c = \frac{P_n}{\Omega_c}$$
$$= \frac{927 \text{ kips}}{1.67}$$
$$= 555 \text{ kips}$$

$$M_c = \frac{M_n}{\Omega_c}$$
$$= \frac{579 \text{ kip-ft}}{1.67}$$
$$= 347 \text{ kip-ft}$$

Because $P_r/P_c > 0.2$, the AISC 360-16 unity check value is:

$$\frac{P_r}{P_c} + \frac{8}{9}\left(\frac{M_r}{M_c}\right) = \frac{210 \text{ kips}}{555 \text{ kips}} + \frac{8}{9}\frac{(185 \text{ kip-ft})}{(347 \text{ kip-ft})}$$
$$= 0.852$$

Case of *H* = 2%*P*

***Code Check Using the 1989 AISC* Specification**

The load demands at the base of the cantilever are taken from Table 4:

$P_r = 300$ kips
$M_r = 90$ kip-ft

The applied axial and bending stresses are then calculated as follows:

$$f_a = \frac{P_r}{A_g}$$
$$= \frac{300 \text{ kips}}{24 \text{ in.}^2}$$
$$= 12.5 \text{ ksi}$$

$$f_b = \frac{M_r}{S_x}$$
$$= \frac{90 \text{ kip-ft}}{123 \text{ in.}^2}$$
$$= 8.78 \text{ ksi}$$

The allowable axial and bending stresses, as well as the factored Euler stress, are identical to the $H = 5\%P$ case—that is:

$F_a = 22.8$ ksi

$F_b = 30$ ksi

$F_e' = 42.3$ ksi

The 1989 *Specification* code unity check value is thus calculated as:

$$\frac{f_a}{F_a} + \frac{C_m f_b}{\left(1 - \frac{f_a}{F_e'}\right) F_b} = \frac{12.5 \text{ ksi}}{22.8 \text{ ksi}} + \frac{0.85(8.78 \text{ ksi})}{\left(1 - \frac{8.75 \text{ ksi}}{42.3 \text{ ksi}}\right)(30 \text{ ksi})}$$
$$= 0.901$$

Code Check Using the AISC 360-16 ELM

The load demands at the base of the cantilever are taken from Table 4:

$P_r = 300$ kips

$M_r = 114$ kip-ft

As with the $H = 5\%P$ case, the nominal axial and flexural strengths are calculated, based on Equations 9 and 11, to be $P_n = 927$ kips and $M_n = 579$ kip-ft. To be used for ASD, these nominal strengths are reduced by the ASD safety factor Ω_c:

$$P_c = \frac{P_n}{\Omega_c}$$
$$= \frac{927 \text{ kips}}{1.67}$$
$$= 555 \text{ kips}$$

$$M_c = \frac{M_n}{\Omega_c}$$
$$= \frac{579 \text{ kip-ft}}{1.67}$$
$$= 347 \text{ kip-ft}$$

Table 5. Unity Check Ratios for the Cantilever Example		
	1989 *Specification*	**AISC 360-16**
$H = 5\%P$	0.932	0.852 (–8.6%)
$H = 2\%P$	0.901	0.832 (–7.7%)
Note: % change is measured against the 1989 *Specification* UC value.		

Because $P_r/P_c > 0.2$, the AISC 360-16 code check value is:

$$\frac{P_r}{P_c}+\frac{8}{9}\left(\frac{M_r}{M_c}\right)=\frac{300\text{ kips}}{555\text{ kips}}+\frac{8}{9}\frac{(114\text{ kip-ft})}{(347\text{ kip-ft})}$$
$$=0.832$$

Unity Check Summary for the Cantilever Example

The code unity check (UC) values for the cantilever example are summarized in Table 5. For the $H = 5\%P$ case, bending has a larger UC component than axial force. For the $H = 2\%P$ case, the situation is reversed with the axial force having a larger UC component than bending. However, this has only a minor effect on the relative UC between the 1989 AISC *Specification* and AISC 360-16, as shown in Table 5. The AISC 360-16 UC values are lower than the 1989 *Specification* values by approximately 8%. This is first because the 1989 *Specification* flexural capacity is typically lower than AISC 360-16. The 360-16 flexure strength considers the combination of torsional and warping rigidities, while the 1989 *Specification* only considers the larger of the two. The second reason that 360-16 tends to be lower is due to the 8/9 factor in Equation 7. In the 1989 *Specification* beam-column buckling equation, Equation 1, this factor does not exist.

DESIGN EXAMPLE 2

Given:

Perform code checks for the 2D jacket structure, as shown in Figure 3, at the top of a portal tubular column where the highest bending moment occurs. The tubular column has the following geometric and material properties:

36 in. × 1 in.
A_g = 110 in.^{2}
I = 16,851 in.^{4}
S = 936 in.^{3}
r = 12.3 in.
E = 29,000 ksi
F_y = 50 ksi
L = 33 ft

The following parameters also apply to the column:

K = 1.8 (AISC *Manual*, 9th Ed, ELM)
K = 1.0 (DM, FOM)
C_m = 0.85

The column loading is as follows:

P = 2,600 kips
q = 4 kips/ft
Total vertical load $V = P + 2q$ (74.7 ft)
Total horizontal load $H = 2\%V$

The portal frame columns are tubular members; hence, API RP-2A provisions will be used in their design. The code checks to be performed are thus not truly AISC *Specification* checks but are similar. In API RP-2A, the analysis approach and

beam-column resemble the AISC *Specification* equations, but the tubular allowable stresses are taken from the API RP-2A WSD provisions.

A Note on the *K*-Factor

A recently published paper by Ku et. al. (2020) discussed the various *K*-factor calculation procedures for portal frame columns. For the 2D structure considered in this example, the portal column *K*-factor has the following values from different analysis methods:

AISC *Specification* unbraced alignment chart:	$K = 2.45$
Ku et. al. (2020):	$K = 1.69$
ABAQUS FEM Solution:	$K = 1.78$

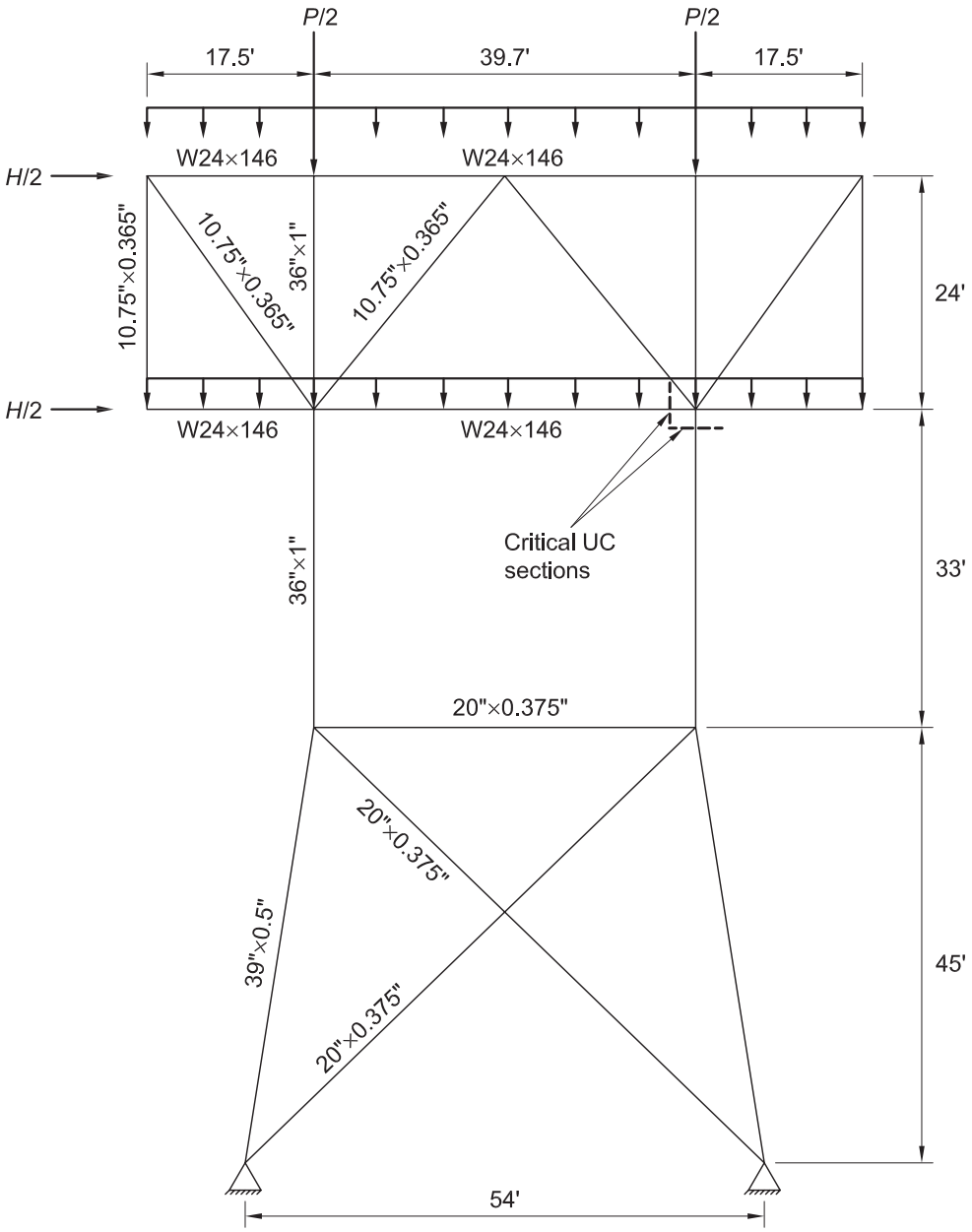

Fig. 3. Two-dimensional offshore jacket.

Table 6. First- and Second-Order Loads for the 2D Jacket Example ($H = 2\%V$)			
	P_r (kips)	M_r (kip-ft)	B_2
First order	1,650	642	—
Second order (ELM)	1,660	808	1.35
Second order (DM)	1,660	869	1.41
First order (FOM)	1,660	897	—

The AISC *Specification* unbraced alignment chart applies to a moment frame, which is completely unbraced throughout the height of structure. For a jacket portal frame, it is combined with a braced topside from above and a braced jacket from below. Thus, the assumption of a complete moment frame results in a *K*-factor that is too conservative. Ku et. al (2020) provides a new analytical *K*-factor solution based on the braced-unbraced-braced configuration. This analytical solution was derived by using slope-deflection equations coupled with stability functions that results in an improved *K*-factor estimate for portal columns. In the following, $K = 1.8$ will be used in all code checks that require a *K*-factor (i.e., $K \neq 1$).

Load Analysis

The general-purpose finite element analysis software ABAQUS (2018) was used to determine the first- and second-order member loads and joint deflections. Each of the portal frame columns is discretized into eight 2-node beam-column elements. Other structural components of the 2D topsides and jackets are discretized with meshes of similar size.

The portal column loads from the ABAQUS analyses are shown in Table 6. For the second-order analysis, the external loads need to be magnified by the $\alpha = 1.6$ factor for response calculations. The member loads thus obtained are then divided by the α factor for member code checks. In lieu of second-order analysis, the $B_1 - B_2$ method coupled with first-order structural analysis can also be used to obtain the second-order loads. Accurate second-order loads similar to the Table 6 numbers can be obtained from the $B_1 - B_2$ method; see IntelliSIMS (2019a, b).

First-Order Load

The first-order column loads are obtained from the first-order structural analysis using nominal *EA* and *EI*, with the external loads given in Figure 3.

Second-Order (ELM) Load

The second-order ELM column loads are obtained from the second-order structural analysis using nominal *EA* and *EI*, with the external loads given in Figure 3 multiplied by $\alpha = 1.6$. After the second-order structural analysis, the resulting member loads are divided by $\alpha = 1.6$ and used for design. With reference to Table 2, the ELM method can only be used when $B_2 \leq 1.5$. This is confirmed by Table 6 in which the B_2 factor is calculated as 1.35. Also, from Table 2, a minimum notional load of $0.2\%V$ needs to be considered. Because the actual lateral load applied is $2\%V$, this minimum notional lateral load does not apply.

Second-Order (DM) Load

The second-order DM column loads are obtained from the second-order structural analysis using $0.8EA$ and $0.8EI$, with the external loads given in Figure 3 multiplied by $\alpha = 1.6$. After the second-order structural analysis, the resulting member loads are divided by $\alpha = 1.6$ and used for design. The following portal column axial load ratio is checked:

$$\frac{\alpha P_r}{P_y} = \frac{1.6(1{,}660 \text{ kips})}{(50 \text{ ksi})(110 \text{ in.}^2)}$$
$$= 0.48 \leq 0.50$$

Hence, no further stiffness reduction of the portal columns is required; see Table 2. The minimum notional load of $0.2\%V$ does not apply since the actual lateral load is $2\%V$, for the case of $B_2 \leq 1.5$.

First-Order FOM Load

The first-order FOM column loads are obtained from the first-order structural analysis using nominal *EA* and *EI*, with the external loads given in Figure 3. An additional lateral load, N_i, must be applied at the top of the portal bay. N_i is calculated as:

$$N_i = 2.1\left(\frac{\Delta}{L}\right)Y_i$$
$$= 2.1\left(\frac{1.1 \text{ in.}}{33 \text{ ft}}\right)(3{,}200 \text{ kips})$$
$$= 29.8 \text{ kips}$$

where Δ is the first-order portal frame interstory drift under the external load in Figure 3, $L = 33$ ft is the portal column length, and Y_i is the total vertical load applied at the portal column bay. $Y_i = V$ in this example. This lateral load, N_i, is "additive"; that is, it needs to apply regardless of the magnitude of actual lateral load. From Table 2, N_i also needs to be checked for:

$$N_i \geq 0.0042\frac{Y_i}{\alpha}$$
$$N_i = 29.8 \text{ kips}$$

$$0.0042\frac{Y_i}{\alpha} = 0.0042\frac{(3{,}200 \text{ kips})}{1.6}$$
$$= 8.39 \text{ kips}$$

which is satisfied.

Validity of the FOM method is limited to cases with member axial load $\alpha P_r/P_y \leq 0.50$. This value was calculated earlier as 0.48; thus, the FOM method can be used. It has been mentioned earlier in this paper that the $H = 5\%V$ case is more likely to be the norm for offshore structures, in which the axial load demand is less than the $H = 2\%V$ case. Because the $H = 2\%V$ case just barely passed the FOM applicability threshold, it can be reasonably expected that the FOM method may be applicable to most offshore structures. The offshore structural designers need to fully understand the various applicability conditions before applying the different stability methods listed in Table 2.

Case of $H = 2\%V$

Code Check Based on the 1989 Specification

The load demands at the top of the portal column are taken from Table 6. Note that the first-order loads need to be used with the 1989 *Specification* check.

$$P_r = 1{,}650 \text{ kips}; \; M_r = 642 \text{ kip-ft}$$

The applied axial and bending stresses are then as follows:

$$f_a = \frac{P_r}{A_g}$$
$$= \frac{1{,}650 \text{ kips}}{110 \text{ in.}^2}$$
$$= 15.0 \text{ ksi}$$

$$f_b = \frac{M_r}{S}$$
$$= \frac{642 \text{ kip-ft}}{936 \text{ in.}^2}$$
$$= 8.23 \text{ ksi}$$

The allowable axial and bending stresses were calculated using Equations 3 and 15:

$F_a = 23.1 \text{ ksi}$

$F_b = 36.6 \text{ ksi}$

The following factored Euler buckling stress is required for code checks:

$$F'_e = \frac{12\pi^2 E}{23(KL/r)^2}$$

$$= \frac{12\pi^2 (29{,}000 \text{ ksi})}{23\left[1.8(33 \text{ ft})/(12.3 \text{ in.})\right]^2}$$

$$= 45.0 \text{ ksi}$$

The 1989 *Specification* unity check value is thus calculated as follows:

$$\frac{f_a}{F_a} + \frac{C_m f_b}{\left(1 - \frac{f_a}{F'_e}\right)F_b} = \frac{15.0 \text{ ksi}}{23.1 \text{ ksi}} + \frac{0.85(8.23 \text{ ksi})}{\left(1 - \frac{15 \text{ ksi}}{45.0 \text{ ksi}}\right)(36.6 \text{ ksi})}$$

$$= 0.935$$

Code Check Using the AISC 360-16 ELM

The load demands at the top of the portal column are taken from Table 6. Note that the second order (ELM) loads are used.

$P_r = 1{,}660 \text{ kips}$

$M_r = 808 \text{ kip-ft}$

The allowable axial and bending stresses are identical to the 1989 *Specification* procedure, with the cross-sectional allowable strengths as:

$F_a = 23.1 \text{ ksi}$

$F_b = 36.6 \text{ ksi}$

$$P_c = F_a A_g$$

$$= (23.1 \text{ ksi})(110 \text{ in.}^2)$$

$$= 2{,}540 \text{ kips}$$

$$M_c = F_b S$$

$$= (36.6 \text{ ksi})(936 \text{ in.}^2)$$

$$= 2{,}860 \text{ kip-ft}$$

Because $P_r/P_c = (1{,}660 \text{ kips})/(2{,}540 \text{ kips}) = 0.653 > 0.2$, the 360-16 *Specification* code check value is:

$$\frac{P_r}{P_c} + \frac{8}{9}\left(\frac{M_r}{M_c}\right) = \frac{1{,}660 \text{ kips}}{2{,}540 \text{ kips}} + \frac{8}{9}\frac{(808 \text{ kip-ft})}{(2{,}860 \text{ kip-ft})}$$

$$= 0.904$$

Code Check Using the AISC 360-16 DM

The load demands for the portal column are taken from Table 6. Note that the second order (DM) loads are used:

$P_r = 1{,}660$ kips

$M_r = 869$ kip-ft

The allowable axial and bending stresses for the DM method are as follows:

$F_a = 26.9$ ksi

$F_b = 36.6$ ksi

An important advantage of the DM method is that the *K*-factor can be taken as 1.0; see Table 2. This results in the axial allowable stress increase from 23.1 ksi to 26.9 ksi, illustrated in Figure 4.

Although the *K*-factor is reduced from 1.8 to 1.0, the increase in allowable stress is less dramatic. This is because for not-too-slender members, the axial capacity is controlled by plastic buckling—that is, a transition region from elastic buckling to full yield. In this region, the member capacity is less sensitive to the change of *K*-factors when compared to the elastic buckling region.

The allowable cross-sectional strengths are calculated as follows:

$$P_c = F_a A_g$$
$$= (26.9 \text{ ksi})(110 \text{ in.}^2)$$
$$= 2{,}960 \text{ kips}$$

$$M_c = F_b S$$
$$= (36.6 \text{ ksi})(936 \text{ in.}^3)$$
$$= 2{,}860 \text{ kip-ft}$$

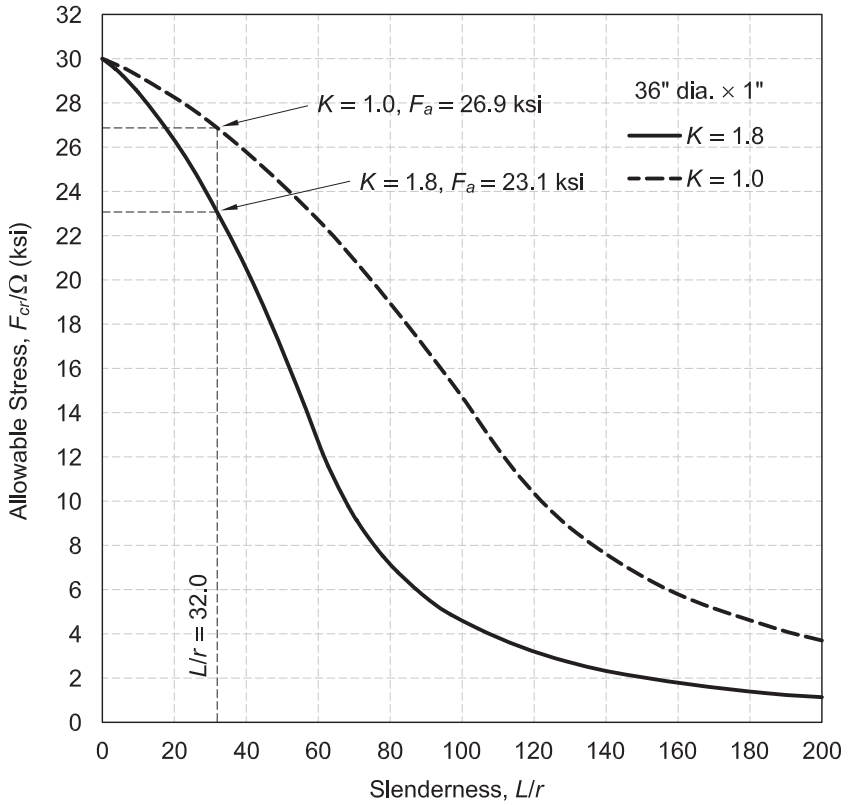

Fig. 4. Axial allowable stress comparison between ELM and DM.

Table 7. Code Unity Check Ratios for the 2-D Jacket Example ($H = 2\%V$)	
	UC Values
1989 AISC *Specification* procedure	0.935
AISC 360-16 ELM procedure	0.904 (–3.3%)
AISC 360-16 DM procedure	0.833 (–10.9%)
AISC 360-16 FOM procedure	0.842 (–9.9%)
Note: % change measured against 1989 AISC *Specification* UC.	

Because $P_r/P_c = (1{,}660 \text{ kips})/(2{,}960 \text{ kips}) = 0.563 > 0.2$, the AISC 360 DM code check value is:

$$\frac{P_r}{P_c} + \frac{8}{9}\left(\frac{M_r}{M_c}\right) = \frac{1{,}660 \text{ kips}}{2{,}960 \text{ kips}} + \frac{8}{9}\frac{(869 \text{ kip-ft})}{(2{,}860 \text{ kip-ft})}$$
$$= 0.833$$

Code Check Using the AISC 360-16 FOM

The load demands at the top of the portal column are taken from Table 6. Note that the first-order (FOM) loads are used.

$P_r = 1{,}660$ kips

$M_r = 897$ kip-ft

The allowable stress and the allowable cross-sectional strengths are identical to the DM case (note that $K = 1$):

$P_c = 2{,}960$ kips

$M_c = 2{,}860$ kip-ft

Because $P_r/P_c = (1{,}660 \text{ kips})/(2{,}960 \text{ kips}) = 0.563 > 0.2$, the 360-16 FOM code check value is:

$$\frac{P_r}{P_c} + \frac{8}{9}\left(\frac{M_r}{M_c}\right) = \frac{1{,}660 \text{ kips}}{2{,}960 \text{ kips}} + \frac{8}{9}\frac{(897 \text{ kip-ft})}{(2{,}860 \text{ kip-ft})}$$
$$= 0.842$$

UC Summary for the 2D Jacket Example

Code unity check values are summarized in Table 7. The comparisons are consistent with the cantilever example of Table 5, with the AISC 360-16 ELM UC value slightly lower than the 1989 *Specification* value. The decrease in UC is slightly less when compared to the cantilever example (–3.3% vs. –7.7%). This can be attributed to the fact that for wide-flange members, the lateral-torsional buckling strength is almost always higher in AISC 360-16 than in the 1989 AISC *Specification*. For tubular members, this difference does not exist.

Further UC reduction from ELM to DM/FOM is also observed in Table 7. Other examples studied in IntelliSIMS (2019a, b) show similar trends. This can be attributed to the fact that the axial allowable stresses are higher in DM/FOM due to $K = 1$, while the bending moment increase (from reduced EA and EI) is relatively low and not enough to offset the axial allowable stress increase. The preceding observations apply to the relatively low B_2 range encountered for typical offshore structures. DM and FOM results are similar, which can be anticipated because FOM is, in fact, a calibrated simplified method from DM. Detailed explanations of this calibration can be seen, for example, in AISC Design Guide 28 (Griffis and White, 2013).

PLANNED AISC-360 ADOPTION PATH

The API AISC-360 Adoption Task Group has generated two technical reports (IntelliSIMS, 2019a, b) as well as training material. Both the technical reports and the training material were designed to raise the offshore industry's awareness on frame stability procedures between the 1989 and 2016 AISC *Specifications*. As discussed in the Introduction, although the API RP-2TOP has adopted AISC 360-10, the relationship between the first- and second-order structural analyses and their distinctly matched beam-column equations have not been fully explained in API RP-2TOP.

The tubular member design equations as contained in API RP-2A WSD and API RP-2A LRFD are based on methodologies consistent with the 1989 AISC *Specification*. The structural analysis is based on the first-order analysis, and the beam-column equation uses a magnification factor for the second-order effect. This governing practice for offshore structures is thus not compatible with AISC 360-16. Therefore, although API RP-2TOP adopts AISC 360, the offshore designers who wish to use RP-2TOP will need to perform both the first- and second-order analyses and then perform member checks in two separate groups (one group for tubular members, and the other for wide-flange and other nontubular members).

The path forward for the offshore structural industry is to continue raising the awareness of the compatibility issue of technical principles. In parallel, addendums and new revisions for API RP-2A and RP-2TOP should be planned to clarify the code check processes. It is envisioned that the frame stability process for the API RP-2A standards will be updated in the next revision for full compatibility with AISC 360.

CONCLUSION

API has discouraged the use of AISC *Specifications* in the past, and only recently (in 2019) partially adopted AISC 360-10 via the publication of API RP-2TOP for the topsides (i.e., deck) designs. The adoption is partial, as RP-2TOP is load and resistance factor design (LRFD) based and is tied to the simultaneously published API RP-2A LRFD 2nd Edition. The traditional method of offshore structural design for U.S. practices has been working stress design, and it will continue to dominate in the foreseeable future. The latest API RP-2A WSD has yet to adopt any AISC *Specification* later than 1989.

In this paper, two examples were discussed in detail regarding their load calculations and code check processes. This paper should be helpful to offshore structural engineers who wish to understand the AISC 360 frame stability procedure. In general, the AISC 360 stability procedure is easy to understand, and its three associated methods (the ELM, DM, and FOM) are straightforward to apply in practice. Structural code checks using the 1989 and 2016 AISC *Specifications* result in similar values, with the 1989 *Specification* slightly on the conservative side. This slight advantage on economy, when switching to the AISC 2016 *Specification*, in terms of weight savings perhaps will be a welcome news to a cost-conscious industry.

API formed a Task Group in 2019 assigned to study the issues associated with AISC 360 adoption. In the immediate future, this Task Group will likely be preparing addendums and/or revisions to existing standards, with the objective of eventual full compatibility with AISC 360.

ACKNOWLEDGMENTS

The authors would like to thank the remaining members of the API AISC-360 Adoption Task Group for their dedication: Boon Sze Tan, Ralph Shaw, Fu Wu, Ben Bialas, Geoff McDonald, Bernard Cyprian, Jay Hooper, Andrea Mangiavacchi, Ian Chu, and Zhaoji Wang. The authors would also like to thank API for the funding it provided to support this study. The opinions expressed in this paper are those of the authors and do not necessarily reflect API's official position.

REFERENCES

ABAQUS/CAE (2018), Dassault Systems Simulia Corp., Johnston, R.I.

AISC (1986), *Load and Resistance Factor Design Specification for Structural Steel Buildings*, American Institute of Steel Construction, Chicago, Ill.

AISC (1989a), *Specification for Structural Steel Buildings, Allowable Stress Design and Plastic Design*, American Institute of Steel Construction, Chicago, Ill.

AISC (1989b), *Steel Construction Manual*, 9th Ed., American Institute of Steel Construction, Chicago, Ill.

AISC (2010), *Specification for Structural Steel Buildings*, ANSI/AISC 360-10, American Institute of Steel Construction, Chicago, Ill.

AISC (2011), *Steel Construction Manual*, 14th Ed., American Institute of Steel Construction, Chicago, Ill.

AISC (2016), *Specification for Structural Steel Buildings*, ANSI/AISC 360-16, American Institute of Steel Construction, Chicago, Ill.

AISC (2017), *Steel Construction Manual*, 15th Ed., American Institute of Steel Construction, Chicago, Ill.

API (1969), *Recommended Practice for Planning, Designing, and Constructing Fixed Offshore Platforms*, 1st Ed., American Petroleum Institute, Washington, D.C.

API (1993), *Recommended Practice 2A-LRFD, Planning, Designing, and Constructing Fixed Offshore Platforms—Load and Resistance Factor Design*, 1st Ed., American Petroleum Institute, Washington, D.C.

API (2014), *Recommended Practice 2A-WSD, Planning, Designing, and Constructing Fixed Offshore Platforms—Working Stress Design*, 22nd Ed., American Petroleum Institute, Washington, D.C.

API (2019), *Recommended Practice 2A-LRFD, Planning, Designing, and Constructing Fixed Offshore Platforms—Load and Resistance Factor Design*, 2nd Ed., American Petroleum Institute, Washington, D.C.

ANSI/API (2019), *Recommended Practice 2TOP*, 1st Ed., ISO 19901-3:2010 (Modified), Petroleum and Natural Gas Industries—Specific Requirements for Offshore Structures—Part 3: Topsides Structure, American Petroleum Institute, Washington, D.C.

Bernuzzi, C., Cordova, B., and Simoncelli, M. (2015), "Unbraced Steel Frame Design According to EC3 and AISC Provisions," *Journal of Constructional Steel Research*, Vol. 114, pp. 157–177.

Carter, C. (2013), *The Evolution of Stability Provisions in the AISC Specification*, SteelDay Eve Presentation, AISC Education Archives, www.aisc.org.

Carter, C. and Geschwindner, L. (2008), "A Comparison of Frame Stability Analysis Methods in ANSI/AISC 360-05," *Engineering Journal*, AISC, Vol. 45, No. 3, pp. 159–170.

Griffis, L.G. and White, D.W. (2013), *Stability Design of Steel Buildings*, Design Guide 28, AISC, Chicago, Ill.

IntelliSIMS (2019a), *AISC-360 Adoption Phase 1 Report*, A Report for API, Revision B.

IntelliSIMS (2019b), *AISC-360 Adoption Phase 2 Report*, A Report for API, Revision A.

Ku, A., Chen, J., and Gunzelman S. (2020), "K-Factor Solution for Combined Braced-Unbraced Offshore Jacket Frames," *Journal of Offshore Mechanics and Arctic Engineering*, Vol. 142, pp. 021703-1-6.

McGuire, W., Gallagher, R.H., and Ziemian, R.D. (2014), *Matrix Structural Analysis*, 2nd Ed., John Wiley & Sons, Inc., New York, N.Y.

Ziemian, R.D. (ed.) (2010), *Guide to Stability Design Criteria for Metal Structures*, 6th Ed., John Wiley & Sons, Inc., Hoboken, N.J.

Investigation of Steel Plate Washer Thickness for Column Anchor Rod Applications

PAUL A. COZZENS, GIAN ANDREA RASSATI, JAMES A. SWANSON, and
THOMAS M. BURNS

ABSTRACT

Since the 13th edition, the AISC *Steel Construction Manual* has included provisions regarding the recommended minimum plate washer thickness used in a column base plate and anchor rod assembly. Each plate washer must have sufficient strength and stiffness to fully develop the anchor rod to which it is fastened without succumbing to pull-through, flexural, or cracking failure. Laboratory tensile testing of an anchor rod, nut, and plate washer assembly was conducted at the University of Cincinnati to study plate washer performance. This testing investigated the capacity of ASTM A572/A572M Grade 50 (ASTM, 2021b) plate washers using the recommended minimum thicknesses as listed in Table 14-2 of the 15th edition of the AISC *Steel Construction Manual* (2017), with anchor rods having ¾, 1, 1½, 2, and 2½ in. diameter. A total of 94 tests were conducted, after which the plate washers were visually assessed for signs of failure, including measurement of permanent out-of-plane deformation. This assessment established that a 40% relative deformation in plate washers could reasonably be judged as a failure threshold due to excessive deformation. Testing and assessment revealed that while 10 plate washers exhibited relative deformations in excess of 40%, the recommended minimum plate washer thicknesses found in AISC *Manual* Table 14-2 were sufficient in fully developing most anchor rods. The notable exception to the current minimum thickness recommendations were for washers in use with anchor rods with diameters of ¾, 1, and 1½ in. made from Grade 105 steel. For these anchor rods, a thicker plate washer than that currently specified is recommended. Testing also found that the anchor rod orientation and the variations of ultimate strength in individual anchor rods did not appear to be significantly associated with the performance of plate washers in these tests.

Keywords: plate washers, pull-through failure, anchor rods, column baseplates, column base connections.

INTRODUCTION

The connection of a column baseplate to the foundation is critically important to the performance and behavior of the framing system. The anchor rods that extend through oversized holes in the steel baseplate are attached through hardened nuts and plate washers covering those holes. The column baseplate connection can be subjected to uplift forces due to high seismic or wind loading conditions that create an overturning moment, placing the anchor rods in tension as the steel baseplate is restrained by the plate washer (Figure 1). Excessive deformation of the plate washer resulting in pull-through failure would cause the actual behavior of the connection to be quite different from the anticipated behavior, which, in turn, could affect the design assumptions. Although the plate washer plays a significant role of the column base connection, there is a lack of experimental research on the behavior and appropriate thickness of plate washers. This lack of guidance regarding column base connections has motivated recent research conducted by Grilli and Kanvinde (2016) at the University of California–Davis, who investigated column base connections subjected to high seismic loads. This experimental study focused on anchor bolts connected by a plate embedded within a concrete footing to compare experimental strength to that predicted by various models. Enhancing knowledge surrounding the behavior of column base connections, including the behavior of plate washers, will help provide guidance in column base connection design and limit the variance between actual and anticipated frame behavior.

The stated purpose of AISC Design Guide 1, *Base Plate and Anchor Rod Design*, is to provide guidance for engineers and fabricators to design, detail, and specify column base plate and anchor rod connections (Fisher and Kloiber, 2006). This reference notes that plate washers can be rectangular, square, or circular, although square washers are the most commonly used because they are easily produced. Proper plate washer behavior should prevent pulling through the hole of the column base plate. Recommended minimum plate washer dimensions, based approximately

Paul A. Cozzens, MSCE, Michael Baker International, Louisville, Ky. Email: paul.cozzens@mbakerintl.com

Gian Andrea Rassati, PhD, Associate Professor, Department of Civil and Architectural Engineering and Construction Management, University of Cincinnati, Cincinnati, Ohio. Email: rassatga@ucmail.uc.edu (corresponding)

James A. Swanson, PhD, Associate Professor, Department of Civil and Architectural Engineering and Construction Management, University of Cincinnati, Cincinnati, Ohio. Email: swansojs@ucmail.uc.edu

Thomas M. Burns, PhD, Adjunct Associate Professor, Department of Civil and Architectural Engineering and Construction Management, University of Cincinnati, Cincinnati, Ohio. Email: burnstm@ucmail.uc.edu

Paper No. 2023-05

Table 1. AISC Design Guide 1, Table 2.3 (Fisher and Kloiber, 2006)

Table 2.3. Recommended Sizes for Anchor Rod Holes in Base Plates

Anchor Rod Diameter, in.	Hole Diameter, in.	Min. Washer Dimension, in.	Min. Washer Thickness, in.
¾	1 5/16	2	¼
⅞	1 9/16	2½	5/16
1	1 13/16	3	⅜
1¼	2 1/16	3	½
1½	2 5/16	3½	½
1¾	2¾	4	⅝
2	3¼	5	¾
2½	3¾	5½	⅞

Notes: 1. Circular or square washers meeting the size shown are acceptable.
2. Adequate clearance must be provided for the washer size selected.
3. See discussion in Section 2.6 regarding the use of alternate 1 1/16-in. hole size for ¾-in.-diameter anchor rods, with plates less than 1¼-in. thick.

on a 3:1 ratio of rod diameter to washer thickness, are given in Table 2.3 of Design Guide 1, shown here as Table 1. The values in Design Guide 1 are an exact match to those given in Table 14-2 of the 15th edition of the AISC *Steel Construction Manual* (2017) shown in Table 2.

Adequate performance of the column base connection depends on the plate washer, whose purpose is to cover the oversized hole in the base plate while transferring any tension forces developed in the anchor rods. Since the second edition of AISC Design Guide 1 was published, changes have occurred to the materials that are commonly specified in base plate design. While ASTM A36/A36M (ASTM, 2019a) steel has been the most common plate material specified in practice for decades, this grade is now becoming obsolete and is not explicitly addressed in the 16th edition of the AISC *Manual* (AISC, 2023). Anchor rods are standardized in ASTM F1554 (ASTM, 2020) and are most commonly specified as Grade 55, although Grades 36 and 105 are typically available (Carter, 1999; Tavarez, 2018). An investigation into the behavior of steel plate washers of varying thicknesses using anchor rods made from all three grades of ASTM F1554 steel is needed to provide further understanding of this critical element.

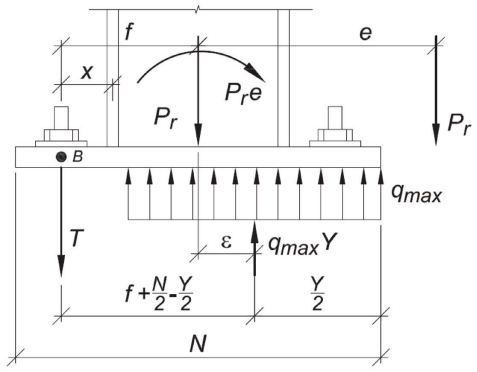

Fig. 1. Anchor rod tension created by large moment (Fisher and Kloiber, 2006).

EXPERIMENTAL TESTING

The main objective for this study was to experimentally evaluate a selected sample of ASTM A572/A572M Grade 50 (ASTM, 2021b) plate washers in conjunction with its appropriately sized ASTM F1554 Grades 36, 55, and 105 threaded rods. This included loading the assembly of specimens to failure, followed by a visual observation of the plate washer failure modes and measurement of the plate washer deformation normal to the tensile loading. A secondary objective was to observe the behavior of the F1554 anchor rods. This included noting discrepancies between the minimum yield criteria and observed yield points; any discrepancies between the minimum and maximum ultimate tensile strengths; and the observed tensile strengths for five diameters of anchor rod, ranging in size from ¾ in. to 2½ in. diameter.

Experimental testing consisted of the tensile loading of 90 sets of specimens, which included one plate washer and one 48-in.-long fully threaded anchor rod. Rods of five different diameters were tested (¾, 1, 1½, 2, and 2½ in.) to provide a representative sample of the diameters listed in AISC *Manual* Table 14-2 (2017). For each of these five

Table 2. AISC *Manual* Table 14-2 (AISC, 2017)

TABLE 14–2
Recommended Maximum Sizes for Anchor-Rod Holes in Base Plates

Anchor Rod Diameter, in.	Max. Hole Diameter, in.	Min. Washer Size, in.	Min. Washer Thickness	Anchor Rod Diameter, in.	Hole Diameter, in.	Min. Washer Size, in.	Min. Washer Thickness
¾	1 5/16	2	¼	1½	2 5/16	3½	½
⅞	1 9/16	2½	5/16	1¾	2¾	4	⅝
1	1 13/16	3	⅜	2	3¼	5	¾
1¼	2 1/16	3	½	2½	3¾	5½	⅞

Notes:
1. Circular or square washers meeting the washer size are acceptible.
2. Clearance must be considered when choosing an appropriate anchor rod hole location, noting effects such as the position of the rod in the hole with respect to the column, weld size and other interferences.
3. When base plates are less than 1¼ in. thick, punching of holes may be an economical option. In this case, ¾-in. anchor rods and 1 1/16-in. diameter punched holes may be used with ASTM F844 (USS Standard) washers in place of fabricated plate washers.

anchor rod diameters, a total of 18 plate washers were tested using combinations of three grades of steel for the anchor rods (ASTM F1554 Grades 36, 55, and 105), two anchor rod orientations (centered in the hole and offset in the hole), and three plate washer thicknesses based on proximity to the value given in Table 14-2. The anchor rod orientation variable was used to study the potential effect that rod orientation relative to the plate washer hole (centered versus offset) may have on plate washer performance. In total, six plate washers were tested per grade and rod diameter, corresponding to 18 washers per rod diameter, and overall, 90 specimens were tested. Due to the lack of experimental testing data, the plate washer thicknesses tested using various combinations of anchor rods and steel grades always used plate washer thicknesses, as well as thicknesses greater than, and sometimes less than, those currently recommended in the 15th edition of the AISC *Manual* in Table 14-2, in order to explore the testing space. At the conclusion of this phase of testing, it was noted that five anchor rods had not achieved their ultimate tensile strength as specified in the ASTM standard. All five rods were Grade 105, and three of those five were 1½ in. diameter. For this reason, four more 1½-in.-diameter Grade 105 threaded rods were acquired along with four accompanying plate washers, with ½ in. and ⅝ in. thicknesses, resulting in a total of 94 sets of specimens tested.

All testing occurred in the High Bay Structural Research Laboratory at the University of Cincinnati. Testing was conducted using a Tinius-Olsen Super L universal testing machine shown in Figure 2. This testing apparatus has top and bottom crosshead plates that are responsible for applying tension force to the assembly using a servo-controlled hydraulic cylinder.

The experimental set-up consisted of two 1½-in.-thick ASTM A572/A572M Grade 50 reaction plates affixed to the testing apparatus using four ¾ in. high-strength bolts—one to the top surface of the top crosshead and one to the bottom surface of the middle crosshead. The bottom plate represented the configuration of a base plate in the anchor rod assembly and had a hole diameter as found in AISC *Manual* Table 14-2. Neither top nor bottom plate deformed significantly during testing. To ensure that these plates did not incur excessive damage during testing, while also fulfilling the provisions regarding base plate hole sizes, the reaction plates were changed for each rod diameter to a plate with an appropriately sized hole. For the top reaction plate, the hole was fabricated 1/16 in. larger in diameter than the anchor rods for the ¾ in. rod, and ⅛ in. larger in diameter for all other rod sizes. The bottom reaction plate was fabricated with a central hole of the diameter given in AISC *Manual* Table 14-2. The top and bottom reaction plates are shown in Figure 3. Additionally, the bottom plates were detailed with short-slotted mounting holes to allow the installation of the plates so that the effect that anchor rod orientation (centered versus offset) may have on plate washer behavior could be investigated (Figure 4).

Each test included one ASTM F1554 anchor rod and one ASTM A572/A572M Grade 50 plate washer with ASTM A563/A56M (ASTM, 2021a) Grade DH nuts fastening the plate washer to the anchor rod and the reaction plates. An ASTM F436/436M (ASTM, 2019b) washer was placed between the top nut and reaction plate.

Once the test specimens were set in place, testing commenced with force and displacement measured over time. The specimens were loaded at a predetermined rate of displacement to ensure that only static force effects were

Fig. 2. Tinius Olsen Super-L universal testing apparatus.

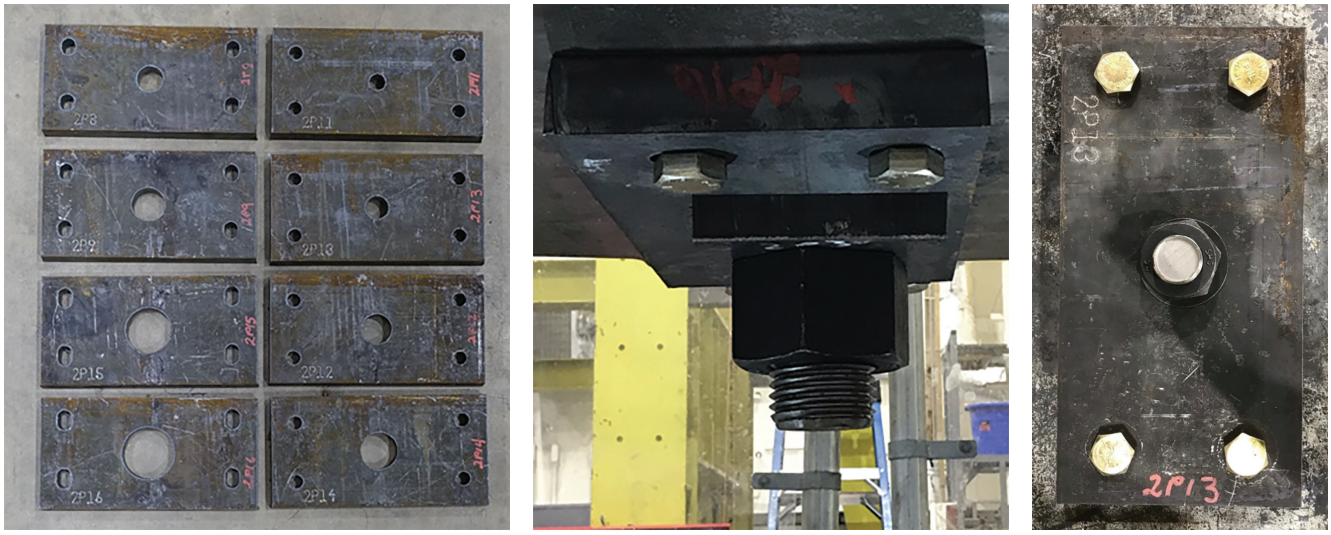

(a) Before testing *(b) Bottom during testing* *(c) Top during testing*

Fig. 3. Reaction plates.

considered. These rates were 0.1, 0.25, 0.5, and 1.0 in./s. Each test began at the lowest rate of displacement, with the rate being increased after yielding was deemed to have occurred, dependent on the stiffness and ductility of each member. The specimens were loaded either to failure of the anchor rod, or to the full capacity of the Tinius-Olsen Super L universal testing apparatus, which has a maximum load capacity of 400 kips. The only anchor rods that exceeded this 400-kip capacity were those rods having a 2½ in. diameter and composed of Grade 105 steel. Once all test data was recorded, it was compiled into force-displacement curves.

DEFORMATION AND VISUAL ASSESSMENT OF PLATE WASHERS

Because there is no direct way during testing to measure the deformation of the plate washers normal to the plane of loading, the measurement of plate washer deformation occurred after the tensile testing had been completed. The deformation for each washer was measured using an electronic dial gauge having a 1 in. stroke affixed to a handcrafted wooden stage. The stage had a dowel rod that held the dial gauge and was fastened to vertical posts at each corner. A top brace was used to ensure the plumbness of the posts and that the stage was horizontal. The apparatus was inspected using a bubble level before each measurement of tested plate washers as shown in Figure 5.

Prior to measuring the plate washer deformation, the thickness of each washer was measured using a digital dial caliper at the mid-point of all four sides, and the average of these four thicknesses was recorded as the average thickness of the washer after the test (Figure 6). In general, this average thickness was found to be within 3% of the nominal washer thickness and averaged less than a 1% deviation from the nominal value in the 94 plate washers measured.

Once the average measured thickness of the washer had been determined, the washer was placed on the stage to determine the location of the absolute minimum elevation on the face of the plate washer. When the location of minimum elevation had been found, the dial gauge was zeroed, and the plate washer was moved along the stage, maintaining contact between the stage and washer at all four corners. This allowed the point of maximum deformation on the plate to be captured by the dial gauge and recorded.

Because the experimental testing in this study used plate washer thicknesses ranging from ¼ in. to 1½ in., a relative deformation was used as a plate washer performance metric. The relative deformation of each washer was calculated as the percentage of absolute maximum deformation to the average thickness of each plate washer tested. Figure 7

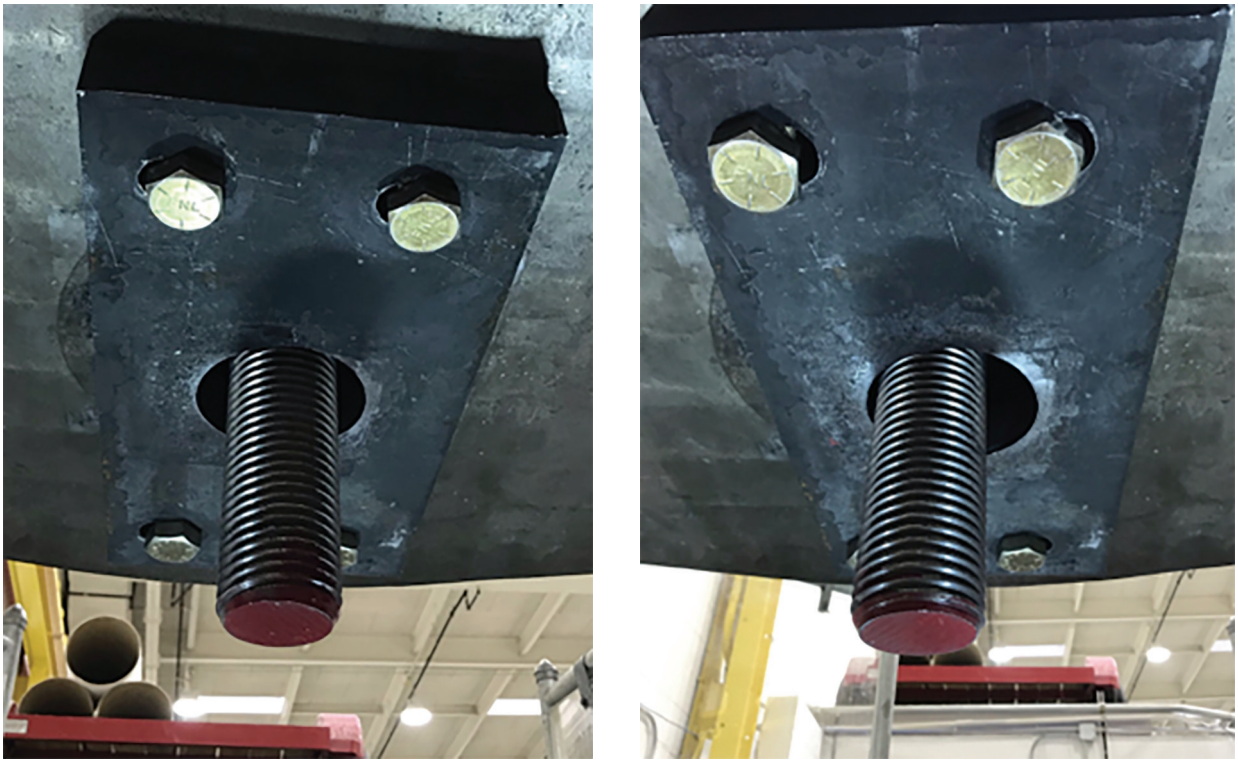

(a) Centered *(b) Offset*

Fig. 4. Anchor rod orientations.

Fig. 5. Assembly of stage and affixed dial gauge.

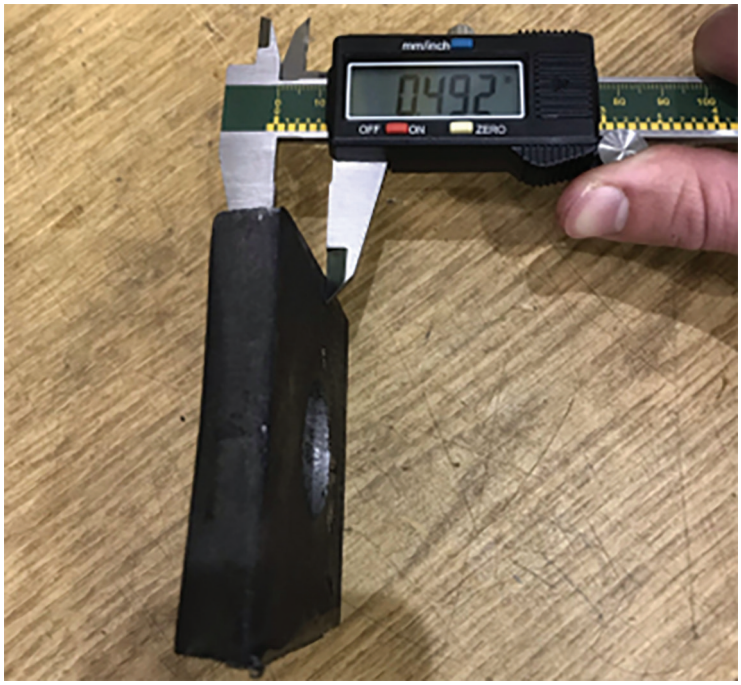

Fig. 6. Measurement of thickness using dial caliper.

shows this data distributed across the entire dataset, which is found in the testing report prepared for the AISC (Cozzens et al., 2021). Further information is provided in the Appendix. Most plate washers exhibited minor to moderate relative deformation. Over half of those tested experienced less than 10% relative deformation, and over three-quarters exhibited less than 20% relative deformation. Of the 10 plate washers that deformed over 40%, nine of those were the thinnest tested, with nominal thicknesses of ¼ or ⅜ in.

To establish the amount of deformation that constitutes failure in a plate washer, a visual assessment of each plate washer was conducted. Those plate washers with only a light amount of deformation were placed in Category 0—Did Not Fail. Plate washers that were judged to have sustained severe deformation were assigned to Category 3—Clear Failure. Two other categories were created (1—No Likely Failure and 2—Likely Failure), and 92 plate washers were visually assessed and placed into one of these categories. Two tests that were at least three standard deviations away from the visual classification's mean were removed. Examples of plate washers assigned to each of these four categories are shown in Figures 8 through 11.

Coupling the visual assessment of plate washers with the physical measurement and determination of relative deformation established a lower bound of relative deformation associated with failure. The results in Figure 12 show a clear delineation appearing between plate washers assigned to Category 1 and those assigned to Category 2. Considering the array of plate washer thicknesses evaluated, the grades of steel anchor rods used, and the various anchor rod orientations, there seems to be sufficient evidence that a threshold for likely failure is apparent when the relative deformation of a plate washer exceeds 40%.

ANCHOR ROD STRENGTH AND ORIENTATION

Based on the design principles established in the AISC *Specification for Structural Steel Buildings* (AISC, 2016b), plate washers are responsible for transferring the design load of the anchor rods through the assembly. However, because the anchor rods have significantly more ductility than the plate washers, it is in the best interest of the structure to ensure the failure of the anchor rods occurs before the failure of the plate washers. To establish a safe and conservative hierarchy of failure for the structure, the performance of each plate washer was evaluated with respect to the ultimate strength of the rod it was responsible for developing, not its design strength. As previously mentioned, the testing in this study has established that a failure threshold involving a plate washer can reasonably be associated with a relative deformation exceeding 40%. The relative deformation of the plate washers in this study were determined after the anchor rods had exceeded their ultimate strength, revealing that 10 plate washers were considered to have failed.

Because inherent variation exists within all groups of test specimens, this study considered the possibility that plate

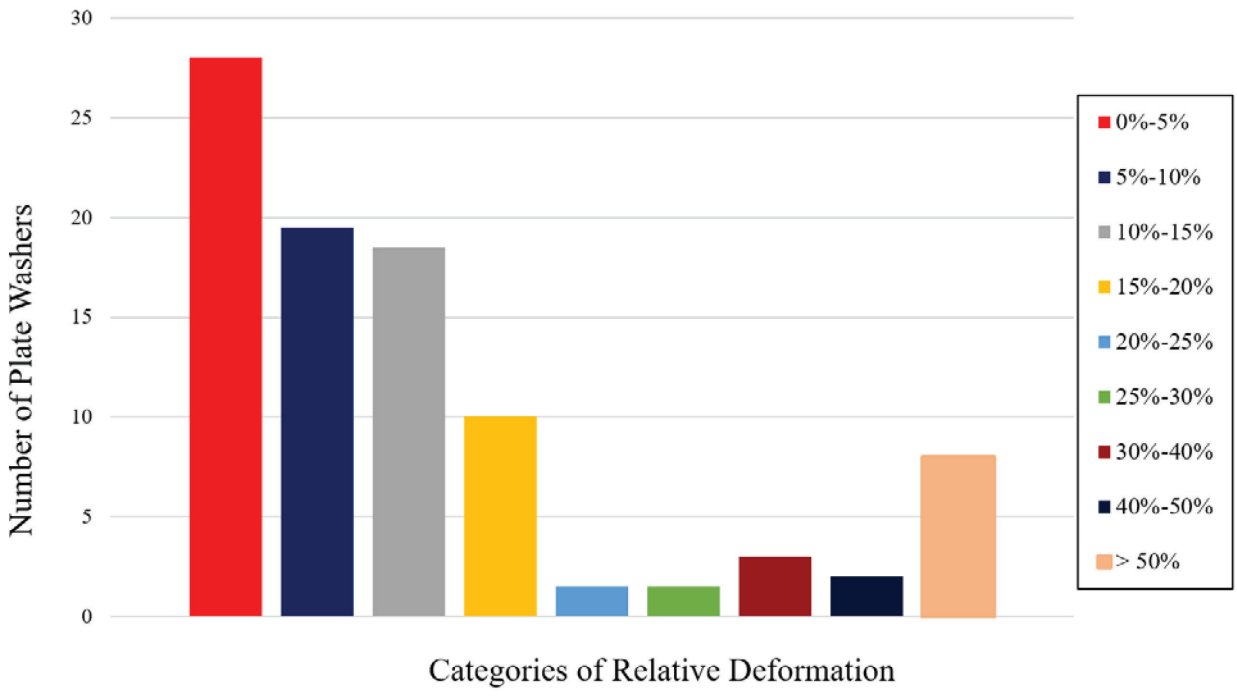

Fig. 7. Distribution of relative deformation of plate washers.

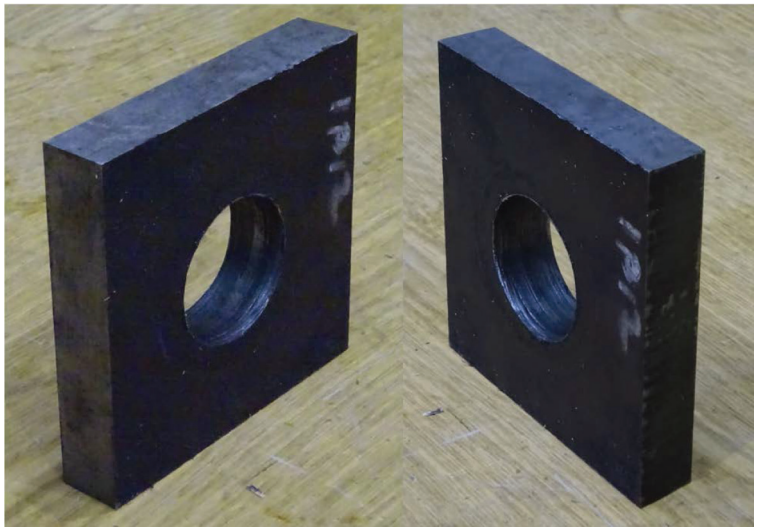

Fig 8. ¾ in. plate washer, centered orientation visual Category 0—did not fail.

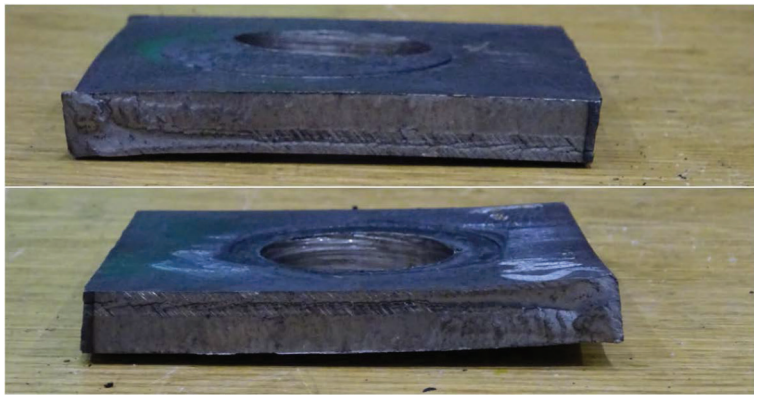

Fig. 9. ½ in. plate washer, centered visual Category 1—no likely failure.

Fig. 10. ¼ in. plate washer, offset orientation visual Category 2—likely failure.

Fig. 11. ¼ in. plate washer, offset orientation visual Category 3—clear failure.

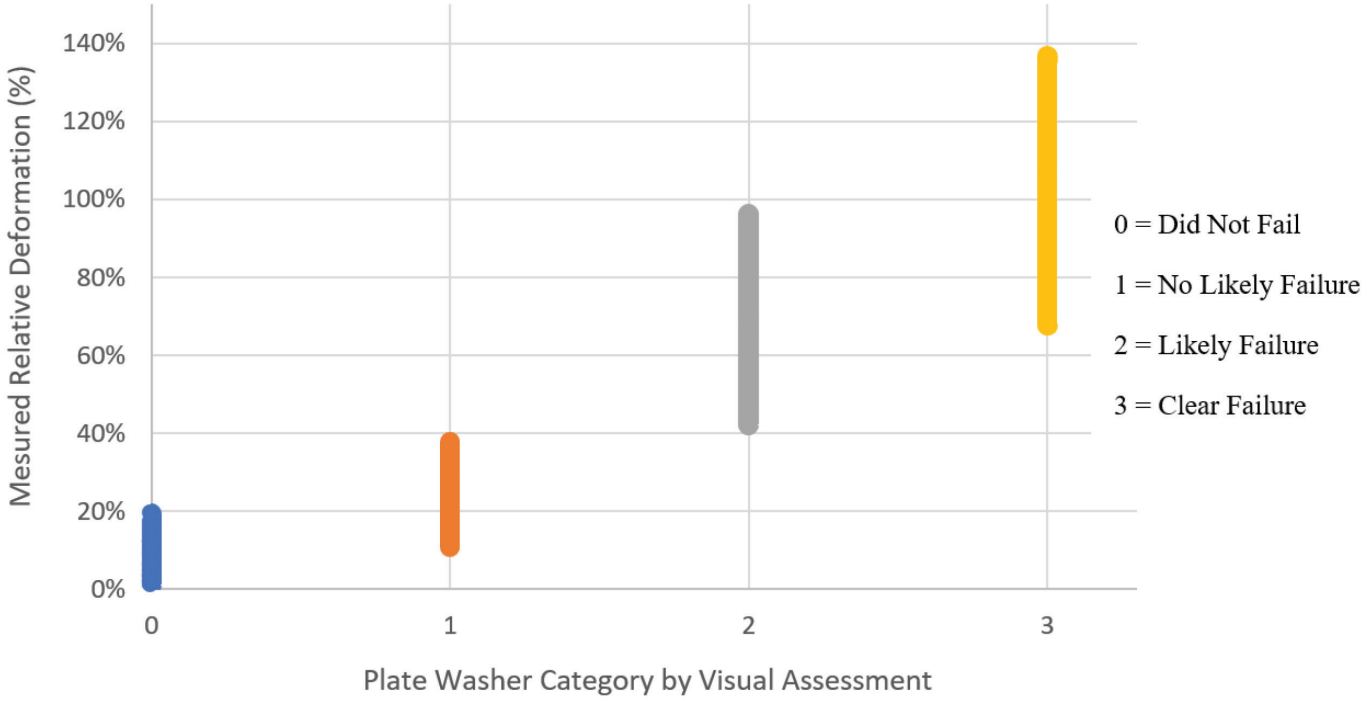

Fig. 12. Visual failure categories and measured relative deformation.

Table 3. ANOVA Results Ratio of Ultimate Rod Capacity to Design Strength				
Groups	Average Ultimate-to-Design Strength Ratio of the Anchor Rods (%)	ANOVA Statistics		
Relative deformation < 40%	154.62	F_{test}	$F_{critical}$	Probability, p
Relative deformation > 40%	154.98	0.004	3.957	0.953

Table 4. ANOVA Results—Orientation of Anchor Rods				
Orientation Groups	Average Relative Deformation of Plate Washer (%)	ANOVA Statistics		
Centered	16.49	F_{test}	$F_{critical}$	Probability, p
Offset	20.71	0.495	3.957	0.484

washer failure may have resulted from an unusual variation between the ultimate strength of individual anchor rods in the group of anchor rods tested. To investigate this possibility, a metric of experimental ultimate strength to design strength of each anchor rod was calculated. This ratio was then compared to the relative deformation of the associated plate washer. A single-factor analysis of variance (ANOVA) was performed on the specimens tested to evaluate the mean ultimate strength to design strength ratio of each anchor rod among two groups—the group of plate washers with a relative deformation greater than 40% (i.e., plate washers that failed) and the group of plate washers with a relative deformation less than 40% (i.e., plate washers that had not failed). This tested a null hypothesis that there was no significant difference in the mean value between the groups using a level of significance of 0.05. The analysis revealed that the mean value of the ratio of ultimate strength to design strength of the failed group versus the nonfailed group were almost identical (154.98 versus 154.62) as was the coefficient of variation (8.1% versus 12%). Not surprisingly, the ANOVA test revealed that the difference in the mean value of the two groups was not significant, with the probability, p, of observing sample results equal to 0.953, which exceeds the stated level of significance. The ANOVA results are shown in Table 3. This suggests that variations in the ultimate strength of individual anchor rods, varying by size and grade of steel, did not appear to have a significant influence on plate washer performance.

Another aspect of this study considered the orientation of the anchor rod relative to the plate washer. The experimental setup allowed for the installation of the plates so that the anchor rod could be placed in a "centered" orientation or an "offset" orientation (i.e., the rod placed to the edge of the plate washer hole). Variations in the designed versus actual location of anchor bolts are an anticipated occurrence and the tolerances governing these variations are found in the AISC *Code of Standard Practice* (AISC, 2016a). As noted earlier, each plate washer was systematically measured after testing to determine its relative deformation.

The anchor rods that were loaded until failure were studied to determine if orientation of the anchor rod (centered versus offset) had any apparent effect on the relative deformation exhibited. Results showed that the mean value of relative deformation for the offset specimens was higher than the group of plate washers having the centered orientation (20.71% versus 16.49%). A single-factor ANOVA was performed to statistically test a null hypothesis that there was no significant difference in the mean value of the centered and offset groups using a level of significance of 0.05. This test revealed that the difference in the mean value of relative deformation for the two groups was not significant, with the probability, p, of observing sample results equal to 0.484, which exceeds the stated level of significance (Table 4). Interestingly, of the 10 plate washers whose relative deformation exceeded the failure threshold of 40%, seven of those were tested in the offset orientation. However, the average relative deformation of those seven specimens having an offset orientation averaged 74.2%, while the relative deformation of washers having the centered orientation was 100.8%. This also supports the statistical finding that anchor rod orientation is not significantly associated with the relative deformation experienced by plate washers.

While the ultimate capacity and orientation of the anchor rods seemed to lack significant association with plate washer performance in this study, a review of the results indicates that stiffness and thickness of the plate washers are influential. As noted previously, only 10 plate washers of the 94 tested exhibited relative deformation above the 40% failure threshold. Of the 10 considered to have failed, six had thicknesses less than the minimum thickness

Table 5. Recommended Plate Washer Thickness—By Rod Diameter Only		
Anchor Rod Diameter (in.)	**Recommended Plate Washer Thickness (in.)**	**AISC *Manual* 15th Ed. Specified Plate Washer Thickness (in.)**
¾	⅜	¼
⅞	½	5⁄16
1	½	⅜
1¼	⅝	½
1½	⅝	½
1¾	¾	⅝
2	¾	¾
2½	⅞	⅞

found in AISC *Manual* Table 14-2. Of the remaining four plate washers that were judged to have failed, all had plate thicknesses matching the minimum thickness found in Table 14-2, but all were part of an assembly using Grade 105 anchor rods. This finding would appear to support the concept of minimum plate washer thickness being associated with the specified grade of steel for anchor rods.

RECOMMENDATIONS

This experimental study considered the behavior of plate washers in a column base connection using anchor rods of various sizes and grades of steel. No plate washers ruptured during testing, but 10 plate washers were unable to effectively develop the ultimate strength of the anchor rods without incurring significant deformations. No clear standard exists currently that would define how much out-of-plane deformation would constitute failure of a plate washer in column base assembly. Based on post-test measurements of the plate washers coupled with visual assessment, it can be reasonably asserted that plate washers experiencing more than 40% out-of-plane deformation relative to its original average thickness can be judged to have failed.

Of the 94 plate washers tested, 10 showed significant out-of-plane deformation exceeding the 40% relative deformation threshold. Of these failed plate washers, six had thicknesses less than that required in the 15th edition of the AISC *Manual* Table 14-2, while the other four plate washers all were coupled with anchor rods using Grade 105 steel. All minimum thicknesses of plate washers in AISC *Manual* Table 14-2 are recommended based on the diameter of the anchor rod only. Because anchors rods made from Grade 105 steel are designed to develop high tensile forces, if minimum plate washer thickness continues to be recommended only based on anchor rod diameter, then the results of this testing support the changes found in Table 5.

The washer thickness recommended for the 2½-in.-diameter rod is ⅞ in. because the ultimate strength of the 2½ in. Grade 105 anchor rod specimens could not be fully developed due to limitations of the testing equipment. This recommendation of ⅞ in. is given tentatively until further testing yields more information.

Although Grade 36 and Grade 55 are more common, anchor rods made from Grade 105 steel may be necessary when conditions warrant the need to develop large tensile forces. As previously noted, 40% of the plate washers that failed in this study had a thickness in line with the minimum thickness specified in AISC *Manual* Table 14-2, but were tested with Grade 105 anchor rods. Given the considerable difference between loads carried by anchor rods of the same diameter, but of different steel grades, it may be valuable to include recommendations by the steel grade of the anchor rod as well as the diameter. The recommended minimum plate washer thickness given in such a format is shown in Table 6.

CONCLUSION

In summary, this study has produced the first experimentally developed values for the thicknesses of plate washers used in column baseplate and anchor rod applications. The results have shown that ASTM F1554 Grade 36 and Grade 55 anchor rods having diameters of ¾, 1, 1½, 2, and 2½ in. can be adequately developed using the currently specified minimum plate washer thicknesses found in Table 14-2 of the 15th edition of the AISC *Steel Construction Manual* (2017). The results also found that for ASTM F1554 Grade 105 anchor rods, the minimum plate washer thicknesses specified in the 15th edition of the AISC *Manual* were not sufficient to develop the rods' ultimate strength without excessive deformations for anchor rods having ¾, 1, and 1½ in., diameters. For anchor rods having ¾, 1, and

Table 6. Recommended Plate Washer Thicknesses—By Diameter and Grade			
Anchor Rod Diameter (in.)	**Grade of Steel**	**Recommended Plate Washer Thickness (in.)**	**AISC *Manual* 15th Ed. Specified Plate Washer Thickness (in.)**
¾	Gr. 36	¼	¼
	Gr. 55	¼	
	Gr. 105	⅜	
⅞	Gr. 36	⅜	5⁄16
	Gr. 55	⅜	
	Gr. 105	½	
1	Gr. 36	⅜	⅜
	Gr. 55	⅜	
	Gr. 105	½	
1¼	Gr. 36	⅜	½
	Gr. 55	½	
	Gr. 105	⅝	
1½	Gr. 36	⅜	½
	Gr. 55	½	
	Gr. 105	⅝	
1¾	Gr. 36	¾	⅝
	Gr. 55	¾	
	Gr. 105	¾	
2	Gr. 36	¾	¾
	Gr. 55	¾	
	Gr. 105	¾	
2½	Gr. 36	¾	⅞
	Gr. 55	¾	
	Gr. 105	⅞	

1½ in., diameters and made of Grade 105 steels, a plate washer ⅛ in. greater in thickness than that currently given in AISC *Manual* Table 14-2 was needed to develop the ultimate strength of the rod without incurring a 40% relative deformation or greater. The currently specified plate washer thickness was found to be sufficient for the 2-in.-diameter Grade 105 anchor rod, and the testing was inconclusive for the 2½-in.-diameter Grade 105 rod. Recommended minimum plate washer thicknesses are provided for anchor rods with ⅞, 1¼, and 1¾ in. diameters using conservative estimates based on the testing conducted. Additionally, it was found that the anchor rod orientation and the potential variations of ultimate strength in individual anchor rods did not appear to be significantly associated with the performance of plate washers in these tests.

Future studies could investigate the performance of plate washers under various conditions including the use of welds, field modification of baseplate holes, and the effect of the combination of shear and tension forces.

REFERENCES

AISC (2016a), *Code of Standard Practice for Steel Buildings and Bridges*, American Institute of Steel Construction, Chicago, Ill.

AISC (2016b), *Specification for Structural Steel Buildings*, ANSI/AISC 360-16, American Institute of Steel Construction, Chicago, Ill.

AISC (2017), *Steel Construction Manual*, 15th Ed., American Institute of Steel Construction, Chicago, Ill.

AISC (2023), *Steel Construction Manual*, 16th Ed., American Institute of Steel Construction, Chicago, Ill.

ASTM (2019a), *Standard Specification for Carbon Structural Steel*, ASTM A36/36M-19, ASTM International, West Conshohocken, Pa.

ASTM (2019b), *Standard Specification for Hardened Steel Washers Inch and Metric Dimensions*, ASTM F436/436M-19, ASTM International, West Conshohocken, Pa.

ASTM (2020), *Standard Specification for Anchor Bolts, Steel, 36, 55, and 105-ksi Yield Strength*, ASTM F1554-20, ASTM International, West Conshohocken, Pa.

ASTM (2021a), *Standard Specification for Carbon and Alloy Steel Nuts (Inch and Metric)*, ASTM A563/563M-21, ASTM International, West Conshohocken, Pa.

ASTM (2021b), *Standard Specification for High-Strength Low-Alloy Columbium-Vanadium Structural Steel*, ASTM A572/572M-21e1, ASTM International, West Conshohocken, Pa.

Carter, C.J. (1999), "Are You Properly Specifying Materials?" *Modern Steel Construction*, March.

Cozzens, P.A., Rassati, G.A., and Swanson, J.A. (2021), *Pull-Through Testing of Plate Washers for Column Anchor Rod Applications*, American Institute of Steel Construction, Chicago, Ill. https://www.aisc.org/globalassets/aisc/research-library/pull-through-testing-of-plate-washer-for-anchor-rod-applications-submitted.pdf

Fisher, J.M. and Kloiber, L.A. (2006), *Base Plate and Anchor Rod Design*, Design Guide 1, 2nd Ed., AISC, Chicago, Ill.

Grilli, D.A. and Kanvinde, A.M. (2016), "Tensile Strength of Embedded Anchor Groups: Tests and Strength Models," *Engineering Journal*, AISC, Vol. 53, No. 2, pp. 87–97.

Tavarez, J. (2018), "Are You Properly Specifying Materials?" *Modern Steel Construction*, April.

APPENDIX

In this Appendix, tables reporting the measured plate washer deformation data, the statistical distribution of relative deformation of the plate washers, and the measured strengths of the threaded rods are presented.

Specifically, Table A-1 summarizes the deformation data of the plate washers tested, reporting the nominal thickness, the measured thicknesses at the mid-points of all four sides, the maximum measured deformation, the average measured thickness, and the percent deformation with respect to both nominal and average measured thickness. Table A-2 contains the binned relative deformation data that was used to produce Figure 7.

Table A-3 summarizes measured data on the threaded rods used during the tests, reporting plate washer orientation (1 = centered, 2 = offset) and its nominal thickness, the rod diameter and grade, its minimum and maximum tensile strength from ASTM F1554, the measured ultimate strength, the minimum yield strength from ASTM F1554, the calculated yield strength (using the 0.2% offset method), and the calculated design strength. Values highlighted in red do not meet some of the ASTM F1554 given limits. Note that the threaded rods used in tests 73 through 78 are consistently above maximum tensile strength, while those in tests 79 through 82 are very close to the minimum tensile strength. It is posited that the rods were mismarked (rod ends are routinely color coded to indicate grade), and thus, the Grade 36 set was really a Grade 55 (and, in this case, the measured values would all be acceptable), and the Grade 55 set was really a Grade 36 (and, in this case, the measured values would be closer to maximum tensile strength, without surpassing it, as would be routinely expected).

The full set of data can be found in the testing report submitted to AISC (Cozzens et al., 2021).

Table A-1. Plate Washer Deformation Data									
Test Number	**Nominal t**	t_1	t_2	t_3	t_4	Δ_{max}	t_{avg}	**% Deformed$_{nominal}$**	**% Deformed$_{ave}$**
1	0.500	0.505	0.495	0.505	0.491	—	0.499	—	—
2	0.500	0.490	0.490	0.489	0.500	—	0.492	—	—
3	0.375	0.375	0.376	0.380	0.370	0.024	0.375	6.32%	6.32%
4	0.375	0.375	0.376	0.372	0.372	0.016	0.374	4.19%	4.20%
5	0.250	0.245	0.246	0.247	0.255	0.062	0.248	24.88%	25.06%
6	0.250	0.242	0.244	0.248	0.254	0.027	0.247	10.76%	10.89%
7	0.500	0.490	0.491	0.502	0.510	0.015	0.498	2.96%	2.97%
8	0.500	0.492	0.501	0.491	0.510	0.086	0.499	17.16%	17.21%
9	0.375	0.369	0.376	0.377	0.375	0.025	0.374	6.67%	6.68%
10	0.375	0.375	0.375	0.369	0.379	0.018	0.375	4.85%	4.86%
11	0.250	0.263	0.248	0.248	0.245	0.051	0.251	20.52%	20.44%
12	0.250	0.242	0.266	0.248	0.249	0.069	0.251	27.64%	27.50%
13	0.500	0.505	0.495	0.505	0.491	0.025	0.499	5.02%	5.03%
14	0.500	0.490	0.490	0.489	0.500	0.046	0.492	9.22%	9.37%
15	0.375	0.375	0.376	0.372	0.376	0.047	0.375	12.53%	12.54%
16	0.375	0.375	0.375	0.374	0.376	0.046	0.375	12.16%	12.16%
17	0.250	0.250	0.252	0.242	0.240	0.177	0.246	70.68%	71.83%
18	0.250	0.241	0.239	0.246	0.248	0.169	0.244	67.44%	69.24%
19	0.500	0.490	0.499	0.493	0.493	0.058	0.494	11.58%	11.73%
20	0.500	0.492	0.492	0.492	0.495	0.059	0.493	11.70%	11.87%
21	0.375	0.374	0.492	0.374	0.375	0.038	0.404	10.11%	9.39%
22	0.375	0.369	0.370	0.368	0.370	0.045	0.369	11.92%	12.11%
23	0.250	0.239	0.245	0.252	0.245	0.240	0.245	96.12%	97.98%
24	0.250	0.248	0.243	0.250	0.253	0.271	0.249	108.36%	109.01%
25	0.500	0.488	0.489	0.493	0.501	0.044	0.493	8.88%	9.01%
26	0.500	0.490	0.492	0.491	0.490	0.053	0.491	10.60%	10.80%
27	0.375	0.371	0.373	0.368	0.370	0.063	0.371	16.80%	17.00%
28	0.375	0.372	0.366	0.372	0.369	0.039	0.370	10.32%	10.47%
29	0.250	0.249	0.250	0.245	0.245	0.342	0.247	136.80%	138.32%
30	0.250	0.245	0.245	0.245	0.241	0.339	0.244	135.48%	138.81%

(Table A-1 continues on the next page)

Table A-1. Plate Washer Deformation Data (continued)									
Test Number	Nominal t	t_1	t_2	t_3	t_4	Δ_{max}	t_{avg}	% $\text{Deformed}_{\text{nominal}}$	% $\text{Deformed}_{\text{ave}}$
31	0.750	0.741	0.744	0.737	0.746	0.020	0.742	2.72%	2.75%
32	0.750	0.739	0.736	0.737	0.747	0.014	0.740	1.85%	1.88%
33	0.500	0.494	0.495	0.498	0.492	0.070	0.495	13.96%	14.11%
34	0.500	0.495	0.491	0.503	0.500	0.068	0.497	13.54%	13.61%
35	0.375	0.373	0.373	0.374	0.375	0.132	0.374	35.07%	35.18%
36	0.375	0.375	0.374	0.375	0.373	0.233	0.374	62.16%	62.28%
37	0.750	0.749	0.749	0.750	0.749	0.023	0.749	3.03%	3.03%
38	0.750	0.751	0.751	0.750	0.749	0.029	0.750	3.91%	3.91%
39	0.500	0.496	0.490	0.486	0.498	0.076	0.493	15.24%	15.47%
40	0.500	0.490	0.491	0.490	0.496	0.078	0.492	15.60%	15.86%
41	0.375	0.372	0.370	0.370	0.378	0.063	0.373	16.77%	16.89%
42	0.375	0.372	0.374	0.374	0.381	0.196	0.375	52.37%	52.34%
43	0.750	0.757	0.749	0.749	0.752	0.027	0.752	3.57%	3.57%
44	0.750	0.750	0.750	0.750	0.751	0.017	0.750	2.24%	2.24%
45	0.500	0.499	0.501	0.493	0.496	0.074	0.497	14.86%	14.94%
46	0.500	0.497	0.497	0.500	0.493	0.096	0.497	19.28%	19.41%
47	0.375	0.372	0.375	0.373	0.373	0.168	0.373	44.85%	45.06%
48	0.375	0.372	0.374	0.370	0.376	0.068	0.373	18.00%	18.10%
49	1.000	1.000	1.005	0.999	0.999	0.022	1.001	2.18%	2.18%
50	1.000	1.001	1.001	1.000	0.999	0.017	1.000	1.68%	1.68%
51	0.750	0.752	0.752	0.751	0.750	0.036	0.751	4.79%	4.78%
52	0.750	0.752	0.752	0.750	0.751	0.043	0.751	5.73%	5.72%
53	0.500	0.490	0.490	0.492	0.501	0.178	0.493	35.52%	36.01%
54	0.500	0.488	0.487	0.498	0.491	0.189	0.491	37.72%	38.41%
1A	0.500	0.498	0.495	0.497	0.495	0.210	0.496	41.94%	42.26%
2A	0.500	0.495	0.495	0.497	0.496	0.069	0.496	13.70%	13.82%
3A	0.625	0.624	0.625	0.625	0.625	0.069	0.625	10.96%	10.96%
4A	0.625	0.624	0.623	0.626	0.625	0.067	0.625	10.72%	10.73%
55	1.000	0.998	0.997	0.991	0.998	0.010	0.996	0.96%	0.96%
56	1.000	1.000	1.000	1.001	1.001	0.014	1.001	1.40%	1.40%
57	0.875	0.880	0.881	0.880	0.886	0.017	0.882	1.93%	1.92%

(Table A-1 continues on the next page)

Table A-1. Plate Washer Deformation Data (continued)									
Test Number	**Nominal t**	t_1	t_2	t_3	t_4	Δ_{max}	t_{avg}	**% Deformed$_{nominal}$**	**% Deformed$_{ave}$**
58	0.875	0.885	0.880	0.880	0.883	0.019	0.882	2.13%	2.11%
59	0.750	0.753	0.754	0.756	0.754	0.011	0.754	1.40%	1.39%
60	0.750	0.755	0.756	0.753	0.752	0.047	0.754	6.32%	6.29%
61	1.000	1.000	1.000	0.998	0.998	0.017	0.999	1.69%	1.69%
62	1.000	1.002	0.999	0.999	1.002	0.060	1.001	5.98%	5.98%
63	0.875	0.883	0.884	0.880	0.881	0.033	0.882	3.73%	3.70%
64	0.875	0.881	0.881	0.882	0.879	0.059	0.881	6.72%	6.68%
65	0.750	0.753	0.753	0.754	0.757	0.051	0.754	6.73%	6.70%
66	0.750	0.753	0.753	0.753	0.757	0.051	0.754	6.81%	6.78%
67	1.250	1.253	1.252	1.253	1.262	0.040	1.255	3.22%	3.20%
68	1.250	1.253	1.256	1.253	1.263	0.044	1.256	3.53%	3.51%
69	1.000	1.003	1.000	1.000	0.998	0.080	1.000	7.96%	7.96%
70	1.000	0.997	0.960	0.999	0.999	0.055	0.989	5.45%	5.51%
71	0.750	0.752	0.753	0.754	0.752	0.122	0.753	16.20%	16.14%
72	0.750	0.754	0.754	0.755	0.756	0.140	0.755	18.68%	18.56%
73	1.000	1.000	1.000	0.999	1.002	0.061	1.000	6.11%	6.11%
74	1.000	1.000	0.999	0.998	1.001	0.046	1.000	4.59%	4.59%
75	0.875	0.883	0.886	0.889	0.887	0.102	0.886	11.61%	11.46%
76	0.875	0.883	0.883	0.883	0.882	0.078	0.883	8.94%	8.86%
77	0.875	0.882	0.882	0.880	0.886	0.075	0.883	8.58%	8.51%
78	0.875	0.882	0.883	0.886	0.882	0.108	0.883	12.33%	12.22%
79	1.000	1.000	0.999	1.001	1.003	0.032	1.001	3.22%	3.22%
80	1.000	1.003	1.002	1.000	1.000	0.044	1.001	4.39%	4.38%
81	0.750	0.755	0.755	0.755	0.757	0.055	0.756	7.36%	7.31%
82	0.750	0.753	0.755	0.757	0.756	0.090	0.755	12.03%	11.94%
83	1.500	1.516	1.515	1.510	1.518	0.017	1.515	1.11%	1.10%
84	1.500	1.507	1.514	1.512	1.514	0.034	1.512	2.26%	2.24%
85	1.250	1.251	1.257	1.253	1.256	0.046	1.254	3.64%	3.63%
86	1.250	1.253	1.253	1.252	1.257	0.043	1.254	3.42%	3.41%
87	0.875	0.882	0.883	0.884	0.882	0.111	0.883	12.66%	12.55%
88	0.875	0.882	0.883	0.883	0.882	0.076	0.883	8.67%	8.60%
89	0.750	0.752	0.755	0.754	0.753	0.075	0.754	9.95%	9.90%
90	0.750	0.755	0.755	0.753	0.754	0.125	0.754	16.71%	16.61%

Table A-2. Statistical Distribution of Relative Deformation											
Stat.	**0%–5%**			**5%–10%**			**10%–15%**			**15%–20%**	
Min	**0.96%**	**0.96%**		**5.02%**	**5.03%**		**10.11%**	**10.47%**		**15.24%**	**15.47%**
Avg.	**2.88%**	**2.87%**		**7.23%**	**7.33%**		**12.00%**	**11.74%**		**17.04%**	**17.13%**
Median	**2.99%**	**3.00%**		**6.73%**	**6.74%**		**11.92%**	**12.02%**		**16.79%**	**16.94%**
Max	**4.85%**	**4.86%**		**9.95%**	**9.90%**		**14.86%**	**13.61%**		**19.28%**	**19.41%**
28	0.96%	0.96%	19.5	5.02%	5.03%	18.5	10.11%	10.47%	10	15.24%	15.47%
	1.11%	1.10%		5.45%	5.51%		10.32%	10.73%		15.60%	15.86%
	1.40%	1.39%		5.73%	5.72%		10.60%	10.80%		16.20%	16.14%
	1.40%	1.40%		5.98%	5.98%		10.72%	10.89%		16.71%	16.61%
	1.68%	1.68%		6.11%	6.11%		10.76%	10.96%		16.77%	16.89%
	1.69%	1.69%		6.32%	6.29%		10.96%	11.46%		16.80%	17.00%
	1.85%	1.88%		6.32%	6.32%		11.58%	11.73%		17.16%	17.21%
	1.93%	1.92%		6.67%	6.68%		11.61%	11.87%		18.00%	18.10%
	2.13%	2.11%		6.72%	6.68%		11.70%	11.94%		18.68%	18.56%
	2.18%	2.18%		6.73%	6.70%		11.92%	12.11%		19.28%	19.41%
	2.24%	2.24%		6.81%	6.78%		12.03%	12.16%			
	2.26%	2.24%		7.36%	7.31%		12.16%	12.22%			
	2.72%	2.75%		7.96%	7.96%		12.33%	12.54%			
	2.96%	2.97%		8.58%	8.51%		12.52%	12.55%			
	3.03%	3.03%		8.67%	8.60%		12.66%	13.61%			
	3.22%	3.20%		8.88%	8.86%		13.54%	13.82%			
	3.22%	3.22%		8.94%	9.01%		13.70%	14.11%			
	3.42%	3.41%		9.22%	9.37%		13.96%	14.94%			
	3.53%	3.51%		9.95%	9.39%		14.86%				
	3.57%	3.57%			9.90%						
	3.64%	3.63%									
	3.73%	3.70%									
	3.91%	3.91%									
	4.19%	4.20%									
	4.39%	4.38%									
	4.59%	4.59%									
	4.79%	4.78%									
	4.85%	4.86%									

Table A-2. Statistical Distribution of Relative Deformation (continued)													
Stat.	**20%–25%**			**25%–30%**			**30%–40%**			**40%–50%**			**>50%**	
Min	20.52%	20.44%		27.64%	25.06%		35.07%	35.18%		41.94%	15.47%		52.37%	52.34%
Avg.	22.70%	20.44%		27.64%	26.28%		36.10%	36.53%		43.40%	17.13%		91.18%	92.48%
Median	22.70%	20.44%		27.64%	26.28%		35.52%	36.01%		43.40%	16.94%		83.40%	84.91%
Max	24.88%	20.44%		27.64%	27.50%		37.72%	38,41%		44.85%	19.41%		136.80%	1338.81%
1.5	20.52%	20.44%	1.5	27.64%	25.06%	3	35.07%	35.18%	2	41.94%	15.47%	8	52.37%	52.34%
	24.88%				27.50%		35.52%	36.01%		44.85%	15.86%		62.16%	62.28%
							37.72%	38.41%					67.44%	69.24%
													70.68%	71.83%
													96.12%	97.98%
													108.36%	109.01%
													135.48%	138.32%
													136.80%	138.81%

Table A-3. Performance of Threaded Rods										
					ASTM Specified		Measured	ASTM Specified	Measured	
Test Number	Orientation	Nominal *t* (in.)	Diameter (in.)	Grade (ksi)	Minimum Tensile (kips)	Maximum Tensile (kips)	Ultimate Tensile (kips)	Minimum Yield (kips)	Yield (kips)	Design Strength (kips)
1	1	0.500	0.750	36	19.4	26.7	23.05	12.00	15.8	14.55
2	2	0.500					22.97		15.8	
3	1	0.375					22.96		15.8	
4	2	0.375					23.02		15.8	
5	2	0.250					23.05		15.8	
6	1	0.250					23.17		16.0	
7	1	0.500	0.750	55	25.0	31.7	29.69	18.40	21.8	18.75
8	2	0.500					29.51		21.6	
9	2	0.375					29.62		22.0	
10	1	0.375					29.65		21.9	
11	1	0.250					29.39		21.5	
12	2	0.250					29.48		21.7	
13	2	0.500	0.750	105	41.8	50.1	48.14	35.10	41.9	31.35
14	1	0.500					47.52		42.2	
15	1	0.375					47.63		41.9	
16	2	0.375					47.54		41.6	
17	2	0.250					48.40		41.5	
18	1	0.250					48.03		41.5	
19	1	0.500	1.000	36	35.2	48.5	47.27	21.80	34.0	26.40
20	2	0.500					47.10		35.2	
21	2	0.375					47.21		35.2	
22	1	0.375					47.17		35.1	
23	1	0.250					46.74		34.5	
24	2	0.250					46.99		35.4	
25	2	0.500	1.000	55	45.4	57.6	51.74	33.30	36.2	34.05
26	1	0.500					51.79		34.0	
27	1	0.375					51.71		35.7	
28	2	0.375					51.73		36.0	
29	2	0.250					51.66		35.7	
30	1	0.250					51.23		35.5	
31	1	0.750	1.000	105	75.8	90.9	76.77	63.60	67.2	56.85
32	2	0.750					84.54		61.8	
33	2	0.500					81.53		70.5	
34	1	0.500					84.41		66.7	
35	1	0.375					76.49		61.8	
36	2	0.375					81.65		70.0	

(Table A-3 continues on the next page)

Table A-3. Performance of Threaded Rods (continued)										
					ASTM Specified		Measured	ASTM Specified	Measured	
Test Number	Orientation	Nominal *t* (in.)	Diameter (in.)	Grade (ksi)	Minimum Tensile (kips)	Maximum Tensile (kips)	Ultimate Tensile (kips)	Minimum Yield (kips)	Yield (kips)	Design Strength (kips)
37	1	0.750	1.500	36	81.5	112.4	104.10	50.60	71.7	81.50
38	2	0.750					113.85		81.8	
39	2	0.500					104.35		82.2	
40	1	0.500					113.66		71.8	
41	1	0.375					103.67		72.8	
42	2	0.375					113.66		81.4	
43	2	0.750	1.500	55	105.0	133.0	119.61	77.30	84.3	78.75
44	1	0.750					119.63		84.5	
45	1	0.500					119.58		83.2	
46	2	0.500					119.82		84.0	
47	2	0.375					119.72		84.0	
48	1	0.375					119.95		83.3	
49	1	1.000	1.500	105	176.0	216.0	190.61	148.00	184.4	132.00
50	2	1.000					174.63		143.0	
51	2	0.750					191.50		143.6	
52	1	0.750					174.27		168.1	
53	1	0.500					191.58		166.1	
54	2	0.500					174.14		143.5	
1A	2	0.500	1.500	105.0	176.0	216.0	197.84	148.00	158.0	132.00
2A	1	0.500					196.87		157.0	
3A	1	0.625					197.45		157.2	
4A	2	0.625					198.42		156.0	
55	1	1.000	2.000	36	145.0	200.0	184.16	90.00	112.0	108.75
56	2	1.000					184.18		113.0	
57	2	0.875					182.86		113.5	
58	1	0.875					184.39		113.5	
59	1	0.750					183.58		114.8	
60	2	0.750					182.89		115.5	
61	2	1.000	2.000	55	188.0	238.0	214.68	138.00	141.0	141.00
62	1	1.000					214.62		141.0	
63	1	0.875					213.97		141.5	
64	2	0.875					213.06		139.5	
65	2	0.750					214.43		140.0	
66	1	0.750					214.79		141.0	

(Table A-3 continues on the next page)

Table A-3. Performance of Threaded Rods (continued)										
					ASTM Specified		Measured	ASTM Specified	Measured	
Test Number	Orientation	Nominal *t* (in.)	Diameter (in.)	Grade (ksi)	Minimum Tensile (kips)	Maximum Tensile (kips)	Ultimate Tensile (kips)	Minimum Yield (kips)	Yield (kips)	Design Strength (kips)
67	1	1.250	2.000	105	312.0	375.0	325.24	262.00	276.5	234.00
68	2	1.250					309.77		271.0	
69	2	1.000					312.46		284.0	
70	1	1.000					323.59		273.0	
71	1	0.750					316.23		284.0	
72	2	0.750					311.86		284.0	
73	1	1.000	2.500	36	232.0	320.0	340.31	144.00	321.0	174.00
74	2	1.000					336.91		318.0	
75	2	0.875					355.52		297.5	
76	1	0.875					357.61		313.0	
77	1	0.875					355.98		315.0	
78	2	0.875					354.39		298.0	
79	2	1.000	2.500	55	300.0	380.0	312.10	220.00	214.0	225.00
80	1	1.000					311.32		217.0	
81	1	0.750					314.29		211.5	
82	2	0.750					312.40		214.5	
83	2	1.500	2.500	105	500.0	600.0	399.41	420.00	—	375.00
84	1	1.500					399.01		—	
85	1	1.250					400.35		—	
86	2	1.250					398.98		—	
87	2	0.875					397.17		—	
88	1	0.875					388.71		—	
89	1	0.750					389.34		—	
90	2	0.750					385.88		—	

Steel Structures Research Update

Innovative Steel Deck System for Highway Bridge Applications

JUDY LIU

INTRODUCTION

Ongoing research on innovative steel bridge decks is highlighted. This study, currently under way at the University of Kansas, is led by Dr. William Collins, Associate Professor in the Department of Civil, Environmental, and Architectural Engineering. Dr. Collins's research interests include fatigue and fracture of metallic structures; bridge design, fabrication, construction, and performance; and evaluation and preservation of historic structures. Among Dr. Collins's accolades are the Robert J. Dexter Memorial Award, a Fulbright Scholar Award to conduct fracture mechanics research in Finland, and the AISC Milek Fellowship. The four-year Milek Fellowship is supporting this research on innovative steel deck systems for highway bridge applications—the first Milek Fellowship project to focus on bridges. Selected highlights from the work to date are presented, along with a preview of future research tasks.

BACKGROUND AND MOTIVATION

Steel decks offer potential benefits but have seen limited use on bridges. Low weight, inherent modularity, and improved durability are among the advantages to using steel bridge decks. High initial costs and challenges with connections and other details are potential barriers to adoption.

Steel bridge decks are typically limited to specific applications. Data from the National Bridge Inventory (NBI) shows that "steel decks are found on less than three percent of the more than 600,000 highway bridges in the United States" (FHWA, 2019). Steel orthotropic decks are most often used on bridges that have self-weight as a major factor in design. These include bridges with a weight constraint, movable bridges, and long-span structures.

Advantages for steel bridge decks include their inherent modularity and their relative light weight. Dr. Collins's conversations with bridge owners reveal that they are interested in deck systems that are easy to fabricate and suited to rapid construction. These discussions align with accelerated bridge construction and other efforts to increase the speed of designing, fabricating, and erecting steel structures (e.g., Mellon et al., 2021; Medlock et al., 2022). Modular construction suits accelerated bridge construction methods, and cost savings can be realized from the reduced construction time. Steel bridge decks are lighter than traditional concrete and precast bridge decks (Mangus, 2005), potentially resulting in reduced superstructure demand for new structures and reduced or eliminated weight restrictions for existing structures. A reduction in weight can also reduce transportation and construction costs.

Steel bridge decks may be a viable option for improved durability as well as performance of bridges in rural areas. Steel decks would not have the issues seen with concrete deck cracking and reinforcing steel corrosion (ASCE, 2017). Meanwhile, the inability to consistently meet material specifications causes issues with concrete in rural areas where mobile batch plants are commonly utilized.

Barriers to adoption of steel bridge decks include fabrication requirements and high initial costs. Past issues with orthotropic bridge deck performance motivated difficult and expensive fabrication requirements (McQuaid and Medlock, 2005). As a result, steel bridge decks are typically more expensive than their conventional cast-in-place and precast bridge decks.

The potential benefits motivate the development of a steel deck system to compete with traditional cast-in-place and precast concrete bridge decks. In addition to cost savings resulting from their light weight and inherent modularity, steel decks could eliminate the need for cross frames and further reduce costs. Steel decks oriented perpendicular to the girder would help with load sharing and potentially replace the cross frames as lateral bracing.

Initial cost, connections, and other details challenge the development of a competitive steel bridge deck system, and any fatigue-prone details must be addressed. Other major considerations include drainage systems, selection of toppings/overlays, barrier rails and their connections to the deck, and panel-to-panel connections. Dr. Collins and his team will address these challenges in their design and evaluation of an innovative, lightweight, modular steel deck system.

Judy Liu, PhD, Research Editor of the AISC *Engineering Journal*, Professor, Oregon State University, School of Civil and Construction Engineering, Corvallis, Ore. Email: judy.liu@oregonstate.edu

PROPOSED RESEARCH AND DELIVERABLES

Dr. Collins's research team has a comprehensive plan to develop a competitive steel deck system. The four-phase plan seeks to create an easy-to-fabricate, lightweight, and modular deck system; address potential barriers to implementation; and produce design recommendations and specifications.

An overarching goal for the research is to develop a steel deck system that is competitive with respect to fabrication cost, life-cycle cost, and structural performance. An additional, expected benefit is the deck system's suitability for rapid construction of a variety of bridge spans and configurations. Specific objectives are to:

1. Develop a steel deck system that is competitive with conventional cast-in-place concrete decks for use in highway bridges. The steel deck system should be lightweight, modular, and easily fabricated from readily available rolled sections.
2. Conduct a comparative life-cycle cost analysis for a highway bridge utilizing the steel deck system and a conventional, cast-in-place concrete deck.
3. Address potential barriers to widespread steel deck adoption through development of critical details and experimental evaluation. Details will include panel-to-panel connections, girder-to-deck connections, and barrier rail connections to the deck. Evaluation will include experimental testing of some connections as well as full-scale panel fatigue testing.

The research is organized into four phases, from literature review to final deliverables. In Phase I, the team surveyed existing steel deck options as well as systems proposed as alternatives to concrete decks. Initial analyses on the two most promising all-steel candidates informed the selection of one steel deck system for further development. Phase II will be focused on design and cost comparison of a bridge with an all-steel deck and one with a conventional cast-in-place concrete deck. The life-cycle cost evaluations will include estimates for fabrication, shipping, erection, scheduled inspections, and maintenance. In Phase III, the research team will conduct analytical and experimental evaluations of the proposed steel deck system. Finite element analysis and a hot spot stress (HSS) approach will be used to study fatigue behavior. The team's plans include physical testing of component-scale and full-scale panels, fatigue tests, and proposed panel-to-panel connection details. Additional testing may be conducted on barrier rail-to-deck or other connections. Phase IV will complete the research with design recommendations and a final research report. The team anticipates proposed changes to design codes and specifications. The research may impact the AASHTO *LRFD Bridge Design Specifications* (AASHTO, 2020); the FHWA *Manual for Design, Construction, and Maintenance of Orthotropic Steel Bridge Decks* (FHWA, 2012); and/or the AASHTO/AWS D1.5 *Bridge Welding Code* (AWS, 2010).

LITERATURE AND EXISTING SYSTEMS REVIEW

The team researched existing bridge deck systems and design criteria. Their literature review summarized the benefits and challenges for existing and proposed deck systems. Additional considerations included bridge components and details such as barriers and their connections to the bridge deck.

Alternative Bridge Decks

The team explored existing concrete, timber, steel and polymer decks. These alternatives present potential advantages and disadvantages, often related to weight, cost, durability, and performance. All provide a comparison and further inform the development of a competitive steel bridge deck system.

Cast-in-place and precast concrete decks may have issues with weight, durability, and performance. As mentioned previously, concrete decks are heavier than the steel decks being considered, and the cast-in-place decks raise concerns about durability and inconsistencies with concrete mixes in rural areas. Precast concrete decks have advantages of controlled casting and curing off site that can be performed in advance and faster construction times with modular, one-way slab, components that can use conventional steel reinforcement or prestressing. However, the connections between precast panels and panels to girders are cast-in-place, adding time and cost to bridge construction.

Timber decks are lightweight but may see limited use on highway bridges due to applicability, performance, and maintenance. Timber decks are typically used for pedestrian bridges and low-volume, short-span vehicular bridges. Different configurations over time have evolved from large sawn stringers with transverse deck logs; to smaller, closely spaced stringers; to longitudinal decks over transverse spreader beams. Nail-laminated decks were once relatively common, but they presented problems related to proper nail placement, warping and nonuniform bearing of decks on the spreader beams, and the resulting uneven load-sharing and crushing of the wood around nails that adversely affected load transfer. Prefabricated decks were developed, moving from nail-laminated to glue-laminated (glulam) members. A challenge with glulam decks is proper shear transfer between adjacent panels. One solution involves passing high-strength steel rods through holes in the deck

panels and post-tensioning the panels together. However, the steel rods must be regularly retensioned due to creep in the wood.

All-steel bridge deck systems such as open grid steel decks and orthotropic decks are good options for temporary structures and bridges needing lightweight decks (Mangus, 2005) but may suffer from poor user experience and high cost. Ride quality and excessive noise are problems noted for open grid decks. Safety concerns include loss of traction on a wet deck surface. Meanwhile, historically poor fatigue performance of orthotropic decks has resulted in stringent design and fabrication requirements, leading to high costs (McQuaid and Medlock, 2005).

Sandwich plate system (SPS) decks were explored but not selected due to cost and durability concerns. The proprietary SPS decks consist of a rigid polyurethane elastomer core and two metal face plates—a steel-fiber reinforced polymer (FRP) composite. In a comparative study, Kennedy et al. (2002) found the performance of SPS decks to be comparable to that of orthotropic steel decks. A benefit for SPS decks is that less welding would be required, presumably resulting in fewer fatigue issues. However, the long-term durability of the SPS decks was in question. It should be noted that all-FRP decks were also explored, given benefits of their light weight and corrosion resistance (O'Connor, 2013). However, these decks raise concerns about long-term durability and degradation of elements exposed to harsh environmental conditions (Kassner, 2004).

Corrugated core steel sandwich panels (CCSSP) present an interesting option with fabrication challenges. The CCSSP decks consist of steel plates with a continuous corrugated core or multiple single-wave channels. CCSSP boast a high stiffness-to-weight ratio (Nilsson, 2017). The panels are fabricated using laser beam welds (LBW) or hybrid-laser arc welds (HLAW) depending on the core configuration. Challenges to CCSSP deck adoption may include obtaining or manufacturing the corrugated core and finding a fabrication facility with the welding capabilities.

Bridge Decks Selected for Further Study

The team selected HSS sandwich panel and inverted WT decks for further study. These two options aligned best with the objectives for a cost-competitive, lightweight, modular deck system utilizing primarily rolled sections. The potential benefits and challenges are summarized.

Selection of an HSS steel sandwich panel deck was based on performance, production, and speed of construction. Rectangular HSS shapes form the core of a sandwich panel with top and bottom plates (Figure 1). Standard, hot-rolled sections already meet ASTM specifications, thus reducing quality-control concerns, and the use of standard shapes facilitates deck production. The HSS were selected over other shapes because of their relatively high shear resistance and torsional rigidity. The structurally efficient HSS sandwich panel deck is envisioned as a prefabricated, modular system that can be designed with minimal field connections to the girders. Passarelli (2011) proposed a shop-welded, field-bolted, grouted deck to girder connection.

Passarelli (2011) investigated laser beam welds (LBW) and hybrid-laser arc welds (HLAW) for the modular HSS panels and recommended HLAW based on the ability to handle fit-up gaps between components and fatigue performance. However, Pasarelli noted that neither weld process is widely adopted. Also, welding within the closed spaces of the sandwich panel creates challenges for fabrication and inspection.

The inverted WT deck system is another selection based on performance, production, and speed of construction. This system uses inverted WT sections with a steel top plate (Figure 2) and was originally developed by Paterson and Hamadani (2021) for railway bridge applications. As with the HSS deck, the use of standard shapes is expected to facilitate production as a prefabricated, modular system. The WTs are fillet-welded to the top plate. Preliminary models by Paterson and Hamadani demonstrated how the WT deck system could be designed to satisfy current design standards. In contrast to the HSS sandwich system, the inverted WT deck is an open system, eliminating any potential limitations for in-service inspections.

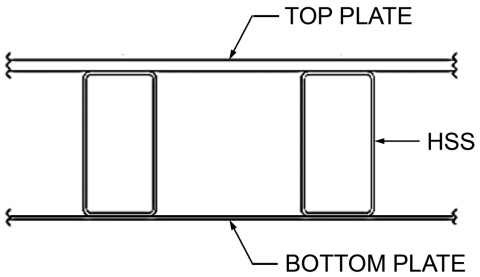

Fig. 1. HSS sandwich panel deck.

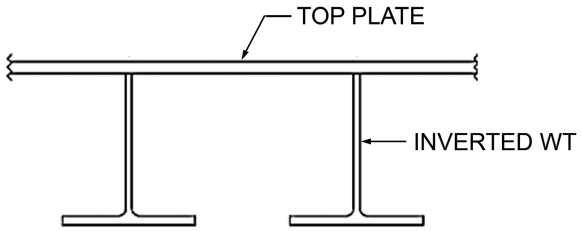

Fig. 2. Inverted WT deck.

Design and Other Considerations

Design criteria and other considerations for construction and in-service performance were gathered by the research team. Deflection limits and maximum allowable fatigue stresses for orthotropic decks were noted (FHWA, 2012). The literature review included types, installation, and maintenance of wearing surfaces. Also considered were types of barriers, their connections to the deck, and performance. Review of these components and their details continues throughout the project, with applicability to the proposed steel deck system.

DECK SYSTEM DEVELOPMENT AND ANALYSIS

The team analyzed the selected HSS and inverted WT decks to inform the sizing of the plates and members. Preliminary models were developed and parametric studies conducted. Fatigue stress and deflection limits helped to define proper member spacing and other dimensions.

The decks were sized to be modular and consistent initially with previous studies. For modular construction, the preliminary 8-ft-wide panel could be delivered to site on a standard truck. Based on Passarelli (2011), HSS8×4×3⁄16 members were used with a ⅝-in.-thick top deck plate and 3⁄16-in.-thick bottom plate. For an inverted WT deck panel with comparable depth and moment of inertia, WT8×20 members and a ⅝-in.-thick top plate were used.

The top plate modeling and loading considered truck wheel loads between members. This study used the front axle load of 16 kips for the HS20 design truck, reduced as appropriate for fatigue limit states (AASHTO, 2020). The wheel loads were simply represented as two 8-kip concentrated loads spaced 6 ft apart. The top plate was modeled as a three-span continuous deck with a 20 in. width corresponding to the HS20 wheel area. For this initial evaluation, a single concentrated wheel load was applied to the center of the interior or end span. The HSS or inverted WT members were modeled as simple supports with center-to-center member spacing ranging from 8 in. to 48 in., in increments of 4 in. Maximum top plate deflections and stresses were recorded for both positive and negative moment regions.

HSS and WT member stresses and deflections were evaluated for the truck loading causing transverse moments in the deck system. The team analyzed a single-span, simply supported deck, and two- and three-span continuous decks. The three deck configurations were loaded with one or more truck axles in various configurations, and girder spacing for these analyses ranged from 8 to 14 ft in 2 ft increments. Positive and negative moment values were considered when evaluating maximum stress and deflection demand.

Top Plate Analyses

Five top plate thicknesses were evaluated along with member spacing. The loading and resulting moment values discussed previously were used to determine the spacing and plate thicknesses needed to satisfy stress and deflection limits (FHWA, 2012). Top plate thicknesses of ½, ⅝, ¾, ⅞, and 1 in. were used for the elastic stress and deflection calculations.

The resulting stresses and deflections were compared for top plate thickness and member spacing for the HSS and inverted WT decks. Figure 3 shows results for top plate stress (ksi) versus member spacing (in.) for an inverted WT deck configuration. A 33 ksi fatigue stress limit (FHWA, 2012) is marked with a dotted line. Top plates that are ⅞ in. or thicker satisfy the limit for all member spacing cases evaluated. Thicknesses of ½, ⅝, and ¾ in. exceed the limit for member spacing of 20, 28, and 40 in., respectively. Top plate stresses are slightly lower for HSS decks because of the shorter clear span. For deflections, similar trends were observed; the ⅞ in. and thicker top plates again satisfied the limit for all member spacing values.

Member Analyses

The HSS and inverted WT members were evaluated primarily for fatigue and serviceability. Yielding, local buckling, and lateral-torsional buckling were also considered for the 14 ft girder spacing and original HSS8×4×3⁄16 and WT8×20 members. Members used in both systems were adequate for these limit states. The preliminary stress analysis focused on a single member of the deck system, neglecting load sharing that may occur. For the deflection analyses, additional member sizes were considered at nominal depths ranging from 6 in. to 10 in., but with weights comparable to that of the original WT8×20 (20 lb/ft). All members satisfied the 10 ksi fatigue stress limit and the deflection limit (FHWA, 2012) for the 8 ft girder spacing, and most all members satisfied these limits for the 10 ft girder spacing. At larger member spacing, an increased moment of inertia due to the top and bottom plate thicknesses was needed for the 12 and 14 ft girder spacing. Stresses and deflections in the HSS deck panels were generally lower than those in the WT. This was attributed to the presence of the bottom plate in the HSS deck panel. Figure 4 shows the trends in deflection (normalized to the deflection limit) versus member spacing for a 12 ft girder spacing. As expected, the decks with deeper members satisfy the deflection limit for a wider range of member spacing.

Panel Weight

Panel weight was also evaluated in a parametric study. Member depth, member spacing, plate thickness, and girder spacing were varied. Nominal member depths again ranged

from 6 to 10 in. for six different HSS and six WT sections. Increments of 4 in. were used for member spacing ranging from 8 to 36 in. Girder spacing of 8, 10, 12, and 14 ft were used. For the HSS deck, top plate thickness was ⅝ in. for member spacing up to 20 in. and then ¾ in. for the others. The inverted WT deck used ⅝ in. top plates for member spacing up to 16 in., ¾ in. for 20 to 28 in. spacing, and ⅞ in. for the 32 and 36 in. spacing. The necessity for top plate thickness differences between the systems was the result of the difference between clear spacing and center-to-center spacing for the different member profiles.

The resulting panel weights were compared for HSS, inverted WT, and comparable reinforced concrete deck. Figure 5 shows a sample graph of panel weight (lb/ft) versus member spacing (in.) for 12 ft. girder spacing. The WT panels are generally lighter than the HSS panels. Some exceptions include panels with 6 in. WT sections and member spacing corresponding to a larger top plate for the WT panel. Larger member spacing, with heavier, but fewer members, typically results in a lighter panel. The majority of the panels evaluated are lighter than a comparable reinforced concrete deck—for example, 800 lb/ft for an 8-in.-thick, 8-ft-wide panel.

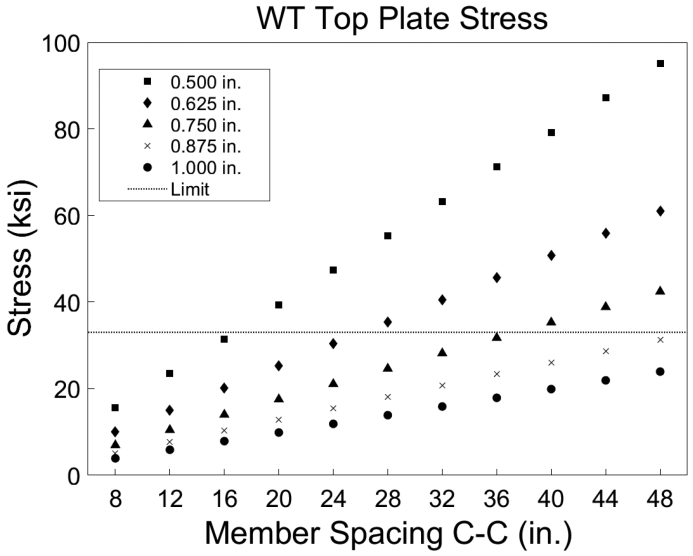

Fig. 3. Top plate stress (ksi) vs. member spacing (in.) for an inverted WT deck panel.

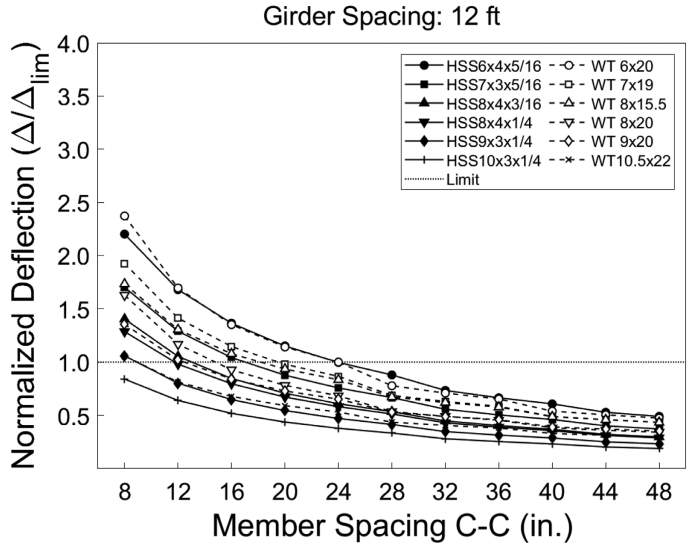

Fig. 4. Normalized deflection versus member spacing for a 12 ft girder spacing.

Evaluation and Selection

The analysis results and practical considerations motivated the choice of the inverted WT deck system. Stress and deflection results were similar for the HSS and inverted WT deck panels. The WT decks tend to be lighter than the HSS panels. The inverted WT is also a more open system with open hot-rolled sections, providing easier access for welding. For these reasons, the research team has moved forward with the inverted WT deck system.

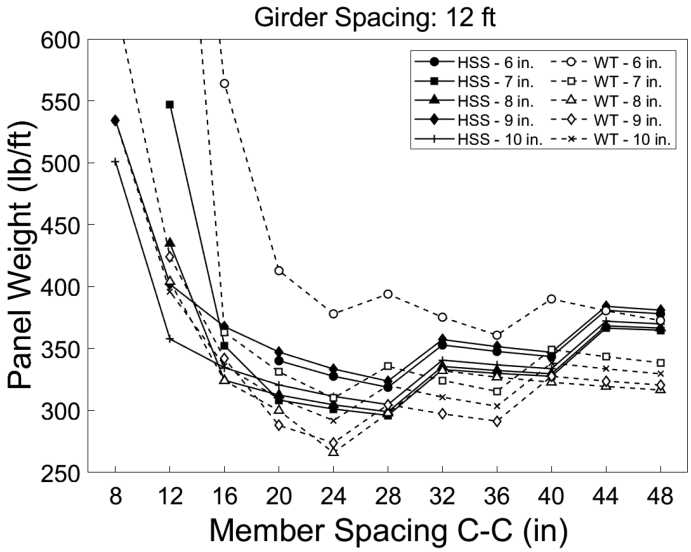

Fig. 5. Panel weight (lb/ft) vs. member spacing (in.) for 12 ft girder spacing.

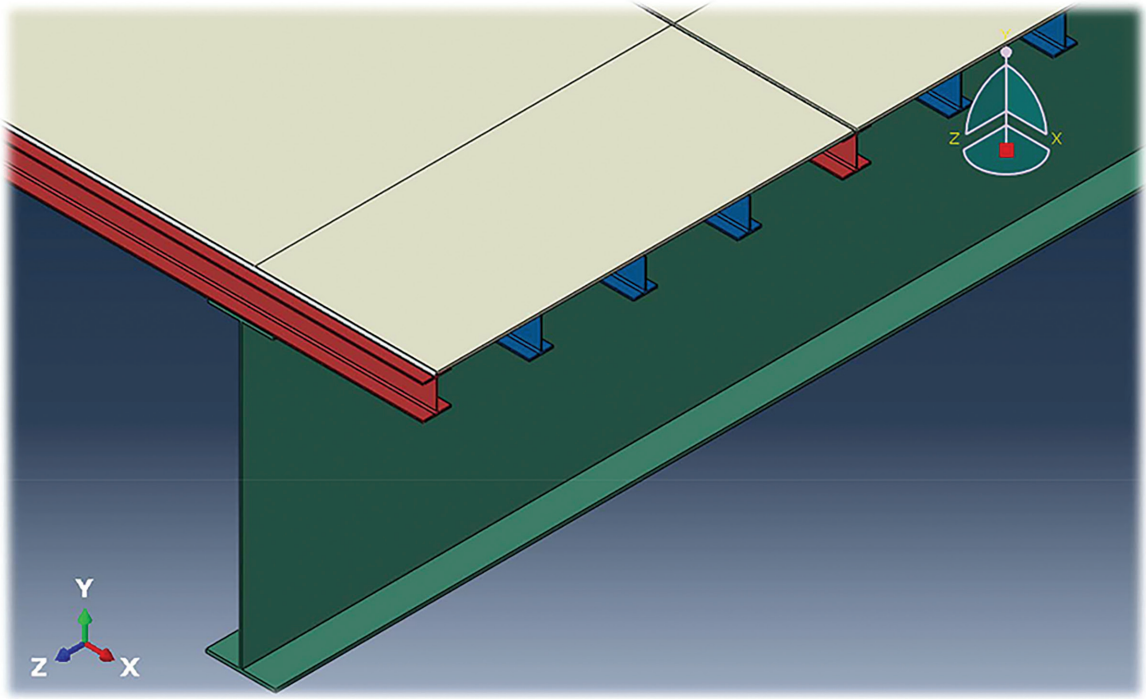

Fig. 6. Preliminary finite element model of a bridge with an inverted WT deck system.

FUTURE WORK

Having addressed the first research objective, the team continues with work on the remaining objectives. The focus will shift from a component level to a system level. Design will be followed by a comparative life-cycle cost analysis of bridges with steel deck and conventional, cast-in-place concrete deck systems. Wearing surfaces, barriers, and connection details will also be addressed. Future work is expected to include finite element (Figure 6), fatigue, and life-cycle cost analyses, as well as physical testing of some connections and full-scale deck panels.

ACKNOWLEDGMENTS

Thank you to Dr. William Collins for his many contributions to this article. Katelyn Davis's contributions as an undergraduate and graduate student researcher are also acknowledged. The research is sponsored by the American Institute of Steel Construction (AISC) through the Milek Fellowship. The researchers would also like to thank Advisory Committee members Calvin Reed, Acting Secretary of Transportation at the Kansas Department of Transportation; Duncan Paterson, Technical Manager at Alfred Benesch & Company; and Ronnie Medlock, Vice President of Technical Services at High Steel Structures. Any findings or recommendations are those of the researchers and do not necessarily reflect the views of the sponsors.

REFERENCES

AASHTO (2020), *LRFD Bridge Design Specifications*, 9th Ed., American Association of State Highway and Transportation Officials, Washington, D.C.

ASCE (2017), *2017 Infrastructure Report Card—Bridges*, American Society of Civil Engineers, Reston, Va.

AWS (2010), *Bridge Welding Code*, 6th Ed., AASHTO/AWS D1.5, American Welding Society, Miami, Fla. www.infrastructurereportcard.org/wp-content/uploads/2017/01/Bridges-Final.pdf (accessed August 2019).

FHWA (2012), "Manual for Design, Construction, and Maintenance of Orthotropic Steel Deck Bridges," FHWA Report No. FHWA-IF-12-027, Federal Highway Administration, Washington, D.C.

FHWA (2019), "National Bridge Inventory (NBI)," Federal Highway Administration, Washington, D.C. https://www.fhwa.dot.gov/bridge/nbi.cfm (accessed August 2019).

Kassner, B.L. (2004), "Long-Term In-Service Evaluation of Two Bridges Designed with Fiber-Reinforced Polymer Girders," MS Thesis, Virginia Polytechnic Institute and State University, Blacksburg, Va.

Kennedy, D.J.L., Dorton R.A., and Alexander, S.D.B. (2002), "The Sandwich Plate System for Bridge Decks," Intelligent Engineering Limited, Ottawa, Ontario, Canada.

Mangus, A.R. (2005), "A Fresh Look at Orthotropic Technology," *Public Roads*, Vol. 68, No. 5, March/April 2005, FHWA-HRT-05-004. https://highways.dot.gov/public-roads/marchapril-2005/fresh-look-orthotropic-technology (accessed December 2023).

McQuaid, D.L. and Medlock, R.D. (2005), "Constructability Issues in Orthotropic Steel Bridge Deck Bridges," *Proceedings of the 2005 World Steel Bridge Symposium*, San Antonio, Tex., March 20–22. https://www.aisc.org/globalassets/nsba/conference-proceedings/2005/mcquaid—2005-wsbs-final.pdf (accessed December 2023).

Medlock R., Russo, F., and vanSalmbrook, D. (2022), "Accelerated Steel: Achieving Speed in Steel Bridge Fabrication," National Steel Bridge Alliance (NSBA), AISC, Chicago, Ill. https://www.aisc.org/contentassets/d42956b27e6b4c618749abe96d687738/nsba-accelerated-steel.pdf (accessed December 2023).

Mellon, D., Kodsuntie, M., Holombo, J., and Rowe, G. (2021), *Accelerated Bridge Construction Manual*, 1st Ed., California Department of Transportation (CalTrans), Sacramento, Calif. https://dot.ca.gov/-/media/dot-media/programs/engineering/documents/abc/ctabc-combined-2021-07-01.pdf (accessed December 2023).

Nilsson, P. (2017), "Laser-Welded Corrugated Core Steel Sandwich Panels for Bridge Application," Chalmers University of Technology, Gothenburg, Sweden.

O'Connor, J.S., (2013), "Composite Bridge Decking: Final Project Report," FHWA Report No. FHWA-HIF-13-029, Federal Highway Administration, Washington, D.C.

Passarelli, G. (2011), "A Feasibility Study on the Fatigue Performance of Laser Beam Welds and Hybrid-Laser Arc Welds Used in a Modular Steel Sandwich Panel Bridge Deck System," MS Thesis, Virginia Polytechnic Institute and State University, Blacksburg, Va.

Paterson, D. and Hamadani, N. (2021), "Low Clearance Steel Ballasted Deck Panels for Rail Bridges," World Steel Bridge Symposium—Virtual, April 12–16.

Guide for Authors

Scope

Engineering Journal is dedicated to the improvement and advancement of steel construction. Its pages are open to all who wish to report on new developments or techniques in steel design, research, the design and/or construction of new projects, steel fabrication methods, or new products of significance to the uses of steel in construction. Only original papers should be submitted.

General

Papers intended for publication should be submitted by email Margaret Matthew, editor, at **matthew@aisc.org**.

The articles published in the *Engineering Journal* undergo peer review before publication for (1) originality of contribution; (2) technical value to the steel construction community; (3) proper credit to others working in the same area; (4) prior publication of the material; and (5) justification of the conclusion based on the report.

All papers within the scope outlined above will be reviewed by engineers selected from among AISC, industry, design firms, and universities. The standard review process includes outside review by an average of three reviewers, who are experts in their respective technical area, and volunteers in the program. Papers not accepted will not be returned to the author. Published papers become the property of the American Institute of Steel Construction and are protected by appropriate copyrights. No proofs will be sent to authors.

Manuscripts

Manuscripts must be provided in Microsoft Word format. Include a PDF with your submittal so we may verify fonts, equations and figures. View our complete author guidelines at **aisc.org/ej**.

Smarter. Stronger. Steel.

American Institute of Steel Construction
130 E Randolph St, Ste 2000, Chicago, IL 60601
312.670.2400 | aisc.org/ej